Award Number: W81XWH-11-1-0814

TITLE: Development of Technologies for Early Detection and Stratification of Breast Cancer

PRINCIPAL INVESTIGATOR: David R. Walt

CONTRACTING ORGANIZATION: Tufts University
Medford, MA 02155

REPORT DATE: October 2014

TYPE OF REPORT: Annual Report

PREPARED FOR: U.S. Army Medical Research and Materiel Command
                               Fort Detrick, Maryland 21702-5012

DISTRIBUTION STATEMENT: Approved for Public Release;
                                             Distribution Unlimited

The views, opinions and/or findings contained in this report are those of the author(s) and should not be construed as an official Department of the Army position, policy or decision unless so designated by other documentation.

REPORT DOCUMENTATION PAGE		*Form Approved* *OMB No. 0704-0188*
Public reporting burden for this collection of information is estimated to average 1 hour per response, including the time for reviewing instructions, searching existing data sources, gathering and maintaining the data needed, and completing and reviewing this collection of information. Send comments regarding this burden estimate or any other aspect of this collection of information, including suggestions for reducing this burden to Department of Defense, Washington Headquarters Services, Directorate for Information Operations and Reports (0704-0188), 1215 Jefferson Davis Highway, Suite 1204, Arlington, VA 22202-4302. Respondents should be aware that notwithstanding any other provision of law, no person shall be subject to any penalty for failing to comply with a collection of information if it does not display a currently valid OMB control number. **PLEASE DO NOT RETURN YOUR FORM TO THE ABOVE ADDRESS.**		

1. REPORT DATE October 2014	2. REPORT TYPE Annual Report	3. DATES COVERED 29 Sept 2013 – 28 Sept 2014
4. TITLE AND SUBTITLE Development of Technologies for Early Detection and Stratification of Breast Cancer		**5a. CONTRACT NUMBER**
		5b. GRANT NUMBER W81XWH-11-1-0814
		5c. PROGRAM ELEMENT NUMBER
6. AUTHOR(S) Prof. David Walt: David.Walt@tufts.edu Prof. Daniel Chiu: chiu@chem.washington.edu Prof. Charlotte Kuperwasser: charlotte.kuper@tufts.edu Prof. Gail Sonenshein: gail.sonenshein@tufts.edu Prof. Rachel Buchsbaum: rbuchsbaum@tuftsmedicalcenter.org E-Mail: david.walt@tufts.edu		**5d. PROJECT NUMBER**
		5e. TASK NUMBER
		5f. WORK UNIT NUMBER
7. PERFORMING ORGANIZATION NAME(S) AND ADDRESS(ES) Tufts University Medford, MA 02155		**8. PERFORMING ORGANIZATION REPORT NUMBER**
9. SPONSORING / MONITORING AGENCY NAME(S) AND ADDRESS(ES) U.S. Army Medical Research and Materiel Command Fort Detrick, Maryland 21702-5012		**10. SPONSOR/MONITOR'S ACRONYM(S)**
		11. SPONSOR/MONITOR'S REPORT NUMBER(S)
12. DISTRIBUTION / AVAILABILITY STATEMENT Approved for Public Release; Distribution Unlimited		
13. SUPPLEMENTARY NOTES		

14. ABSTRACT

The overall goal of this work is to develop ultra-sensitive detection techniques to identify a panel of new biomarkers and indicators with diagnostic and predictive value in breast cancer. This year, multiple ultrasensitive assays for candidate breast cancer biomarkers were developed. Initial screens with commercially purchased samples showed some promising leads with diagnostic potential. Progress has also been made in the area of single cell analysis, which would be useful for analyzing both circulating tumor cells and single cells from tissue biopsies. Circulating tumor cell isolation using microfluidics has been accomplished with multiple platforms and these methods are being refined for high throughput and implementation. Good progress has been made on identifying additional markers (mtDNA, ADAM8, Tiam1) and correlations with various aspects of breast cancer invasiveness are apparent. Finally, a cancer mouse model was developed and a single molecule assay was used to detect a cancer biomarker in the blood after an inoculum of cultured cancer cells that is more than 300 times lower than a conventional inoculation. This bodes well for prospects of being able detect biomarkers in blood for early diagnosis, for monitoring recurrence, or for determining therapeutic efficacy.

15. SUBJECT TERMS

Single molecule detection, cancer biomarkers, ultra-sensitive protein assays, single cells, human-in-mouse model, miRNA, circulating tumor cells

16. SECURITY CLASSIFICATION OF:			17. LIMITATION OF ABSTRACT	18. NUMBER OF PAGES	19a. NAME OF RESPONSIBLE PERSON USAMRMC
a. REPORT	b. ABSTRACT	c. THIS PAGE	UU	40	19b. TELEPHONE NUMBER *(include area code)*
U	U	U			

Table of Contents

<u>**Statement of Work**</u>

The overall goal of this work is to develop ultra-sensitive detection techniques in order to identify a panel of new biomarkers and indicators with diagnostic and predictive value in breast cancer. During years 1 and 2 we will develop ultra-sensitive detection techniques and apply them to identifying prospective biomarkers using the Human-in-Mouse (HIM) model of breast cancer. During years 3-5 we will extend the findings in the HIM model to validate prospective biomarkers in human subjects with breast cancer. This work is broken down into specific tasks by investigator as follows:

INTRODUCTION

Despite the recent advances made in breast cancer diagnostics and treatment, in 2013 the United States is estimated to diagnose approximately 230,000 new cases of invasive breast cancer, resulting in approximately 40,000 deaths.[1] Mammography is a powerful imaging technique for tumor detection; however, it lacks the ability to decipher benign from cancerous tumors, is unable to detect tumors smaller than 1 mm,[2] misses approximately 20% of breast cancers potentially present at the time of screening, and has an 8-10% false positive rate.[3] These drawbacks lead to inaccurate patient diagnosis, which can allow potentially fatal disease progression, or in the cases of over-treatment, unnecessary physical and emotional trauma.[4] ELISA, the most common immunoassay for measuring proteins from breast tumors, excised samples, and serum, has a lower detection limit of ~1-10 pM,[5] which is not sensitive enough to measure low abundance proteins, RNAs, and other biomarkers that could aid in the early and reliable diagnosis of cancer. There is a strikingly clear need to develop techniques capable of detecting biomarkers specific for breast cancer that will enable earlier diagnosis of disease, prediction of patient outcome, and improve therapeutic efficacy in a non-invasive manner. Our goals are to utilize ultrasensitive single molecule techniques developed in our laboratory to discover new biomarkers that meet these requirements within serum so that a simple blood test can be implemented. We are also working to characterize breast cancer biopsy samples with single cell resolution to discover the nature of the underlying heterogeneity in complex cell populations with the goal of correlating disease outcome with genotypes and phenotypes of individual cells.

BODY

<u>**David R. Walt, PhD,**</u> *Tufts University, Department of Chemistry, 62 Talbot Ave, Medford, MA 02155*

Task 1. Develop single molecule diagnostics using HIM (Human-in-Mouse) model (Years 1-2).

1a. Select approximately ten candidate markers (mt DNA, proteins, stem cell markers, etc.) in conjunction with collaborators (Months 1-6).

In conjunction with collaborators, and based on recent literature reports, we have selected a list of candidate biomarkers. The complete list of candidate markers is as follows: EGFRv3, ER-α, ADAM12, LALBA, β-casein, BAG3, BORIS, CA 15-3, CA 19-9, CD49f, CYR61, CDKN2D, CK8/18, DCTN3, GATA3, GRHL3, HER2, KLLN, KIFAP3, LCN2/NGAL, NEDD9, PMS2, PR, RRBP1, SERPINE2, SLUG, SNAIL, TBX3, VPSI3D, and VIM. Additionally, PSA is used as a model biomarker for mouse model and single cell studies since PSA has an established SiMoA.

1b. Develop single molecule assays for the candidate markers selected in 1a. Assays will be developed on microspheres and tested first on standard samples. Assay performance characteristics will be determined to ascertain that they will address concentration ranges of interest and requisite precision. For general protocols see: Nature Biotechnology, 2010, 28, 595-599 (Months 3-15)

In the past year, SiMoA assays have been developed and optimized for several protein biomarkers, including CDKN2D, ADAM12, HER2, CA 15-3, CA 19-9, TBX3, CYR61, LCN2, SERPINE2 and NEDD9. Each developed assay exhibited significantly lower limits of detection compared to commercially available ELISA kits. The following will describe the work performed for each biomarker.

CDKN2D:

Cyclin-dependent kinase inhibitor 2D (CDKN2D) is a member of the INK4 family of cyclin-dependent kinase inhibitors that functions as a cell growth regulator by preventing the activation of CDK kinases. CDKN2D has also been associated with sporadic breast cancer, specifically in triple negative breast patients. This assay has been optimized from a SiMoA LOD of 0.5 pg/mL (28 fM) to 0.1 pg/mL (5.7 fM). The bulk LOD, for comparison, has a LOD of 50 pg/mL.

ADAM12:

ADAM12 is a member of the ADAM (a disintegrin and metalloprotease) protein family that is involved in cell-cell interactions and signaling. ADAM12 expression is associated with tumor growth and metastasis, and is expected to be differentially expressed in breast cancer patients. Successful bulk assays for ADAM12 were developed with a LOD of 3.7 ng/mL. Subsequent optimization for SiMoA detection of ADAM12 yielded a LOD of 3 pg/mL (55 fM).

CA 15-3:

Cancer antigen 15-3 (CA 15-3, or MUC1) is a membrane-bound mucin which protects and hydrates tissues. CA 15-3 is commonly overexpressed and aberrantly glycosylated in cancer patients, inducing cell growth and promoting metastasis. We have successfully developed both bulk and SiMoA assays targeting CA 15-3. The LODs for bulk and single molecule detection of CA 15-3 are 0.04 U/mL and 0.0008 U/mL, respectively. Compared to commercial ELISAs, our SiMoA assay resulted in over a 1000-fold LOD improvement for CA 15-3.

HER2:

Human epidermal growth factor receptor HER2 (also denoted ERBB2 or neu) is a plasma membrane-bound receptor tyrosine kinase known to activate signaling pathways that induce cell proliferation and suppress apoptosis. HER2 is overexpressed in 15-30% of breast cancers and serves as a key biomarker for breast cancer biopsies since targeted drug therapy is available to treat HER2+ cancers. We have developed a SiMoA assay for HER2 in serum exhibiting a LOD of 0.3 pg/mL (2.2 fM). This represents a 50-fold increase in sensitivity compared to commercial ELISA kits.

CA19-9:

Cancer antigen 19-9 (CA 19-9) is expressed on the surface of cancer cells as an oligosaccharide and is traditionally used to monitor pancreatic cancer.[6] It has also been found overexpressed in a number of breast cancers. A sensitive assay has been successfully developed for this marker with a LOD of 0.76 U/mL, a 19x improvement over a typical commercial ELISA kit.

SERPINE2:

SERPINE2 is a serine protease inhibitor that regulates the activity of serine protease urokinase (uPA), which degrades extracellular matrix proteins and promotes cell motility. In advanced breast cancers, uPA is upregulated, facilitating metastatic spread. Interestingly, not much expression of SERPINE2 is reported in normal human mammary tissue, but its expression is found to be elevated in human breast cancers along with the increased expression of uPA.[7,8] Successful bulk assays of SERPINE2 resulted in a LOD of 1.80ng/mL (42.0 pM). Furthermore, SiMoA assays for SERPINE2 yielded a LOD of 36.14 pg/mL (0.864 pM).

NEDD9:

Enhancer of filamentation 1 is a protein that is encoded by the NEDD9 gene and is also known as HEF1 and CASL. NEDD9 is a scaffolding protein that interacts with protein complexes that regulate cell adhesion, migration, division and survival.[9] NEDD9 is frequently overexpressed in many cancer types including breast cancer.[10] Bulk assays of NEDD9 resulted in a LOD of 0.218ng/mL (2.35pM) and subsequent NEDD9 SiMoA assay development yielded a LOD of 16.13pg/mL (174 fM).

Additional Optimizations:

TBX3, CYR61, and LCN2 had previously established SiMoA assays, but these assays have been further optimized in the past year. The TBX3 assay now has a LOD of 1.3 pg/mL (17 fM), while CYR61 can be detected as low as 0.02 pg/mL (0.3 fM—an improvement from 50 fM last year) and LCN2 has a LOD of 0.42 pg/mL (19 fM).

Overall progress on biomarker assay development is summarized in **Table 1**. Table 1 compares the assay sensitivity of commercially available ELISA kits, bulk bead-based assays, and SiMoA assays for each marker.

Table 1. Overall progress summary of breast cancer biomarker assay development.

Biomarker	Bulk LOD		Commercial ELISA LOD		SiMoA LOD		Fold Improvement (based on w/v)
	pg/mL	pM	pg/mL	pM	pg/mL	fM	
ADAM12	3700	67	125	2.3	3	55	40x
BORIS	407	11	78	1.11	10	280	8x
CA 15-3	0.04 U/mL		1 U/mL		0.0008 U/mL		1250x
CA 19-9	58 U/mL		15 U/mL		0.76 U/mL		19x
CDKN2D	51	2.9	10	0.56	0.1	5.7	100x
CYR61	85	1.3	3.8	0.057	0.02	0.3	190x
ERα	130	2	15.6	0.236	0.3	4.5	50x
HER2	665.5	4.8	14.8	0.1	0.3	2.2	50x
LCN2	22	1	40	1.8	0.42	19	100x
NEDD9	463	4.99	1000	10.8	16.1	174	63x
PR	130	1.3	12.5	0.126	0.3	3	42x
SERPINE2	1793	42	78	1.83	36	864	2x
TBX3	211	5.74	116	7.8	1.3	17	89x

1c. Screen blood samples from 'Human-In-Mouse' (HIM) Model obtained from Kuperwasser (Months 12-24). HIM tumors will be created from human breast epithelial cells collected from discarded tissues of women who have undergone reduction mammoplasty surgeries. For more information/details on model: *Nature Protocols*, 2006, 1, 595-599.

We have successfully created a mouse model using low inocula of LNCaP cells to study PSA in mouse serum over time. Through this study, we demonstrated that SiMoA can be used to measure biomarkers in serum prior to tumor formation (see July quarterly report and Kuperwasser section below

for data). These data are currently submitted for publication. Since this study proved that our technique is valid for the early detection of tumors, we chose to pursue the study of clinical samples in lieu of developing more mouse models since this will yield more meaningful data for the end result.

Task 2. Apply single molecule diagnostic technique (developed in Task 1) to analysis of human serum samples (Years 3-5).

2a. Screen clinical samples obtained from Buchsbaum for presence of the markers that could be detected in HIM model (Months 25-30).
      Dr. Buchsbaum has begun consenting patients and collecting clinical samples. These samples will be tested against all available SiMoA assays as they become available. Preliminary experiments have been performed testing human samples using commercially available sources as detailed below in section 2b.

2b. Iterate 2a-2d until a sufficient number of markers has been identified for further investigation. Some candidate markers are expected to either not be found in the clinical samples or will not be predictive of disease state. Other markers may be difficult to measure due to lack of suitable binding reagents. As these markers drop out, others will be added to ensure there is a sufficient number when sample set is expanded (2c) (Months 25-48).
      Breast cancer serum samples and healthy controls were obtained from the commercial supplier BioreclamationIVT. Additionally, urine samples were obtained from the Moses lab at Boston Children's Hospital. These samples were tested with our developed SiMoA assays to quantify the levels of candidate biomarkers in real samples and validate the usefulness of each biomarker. The results are summarized below.

      Validation studies have begun for the candidate biomarkers HER2, ADAM12, CA 15-3, PR, ER-α, CYR61, CA 19-9, and CDKN2D. Serum samples from healthy controls and breast cancer patients were tested to determine if serum concentrations of any of the aforementioned protein biomarkers are indicative of disease states. In the case of HER2 (**Figure 1a**), more data points are required to fully assess its potential as a stand-alone breast cancer serum biomarker. In the case of ADAM12, CA 15-3, PR, and ER-α (**Figure 1b-e**) there is significant overlap between the biomarker concentrations measured in healthy and diseased patients, although the spread of the data is different for each cohort. Finally, the screening results for CYR61, CA 19-9, and CDKN2D seem to have somewhat distinct populations for healthy and breast cancer samples, although there is still overlap within the distribution. The influence of cancer stage, grade, and treatment should also be taken into account. We plan to carry out principal component analysis (PCA) with all of the markers that have been tested in human serum to draw out patterns in the data that may not be immediately apparent. PCA will help guide the selection of a panel of biomarkers that can reliably detect early stage breast cancer.
      Similar screening has been done in urine samples with CYR61 and LCN2 (**Figure 2a-b**). The Moses lab provided breast cancer urine samples and two controls, while additional healthy urine samples were obtained commercially. LCN2 concentrations seem to overlap significantly between healthy and diseased samples, while CYR61 appears to have two different populations whereas diseased urine samples have lower levels of the protein present. More samples will have to be tested to establish expression patterns.
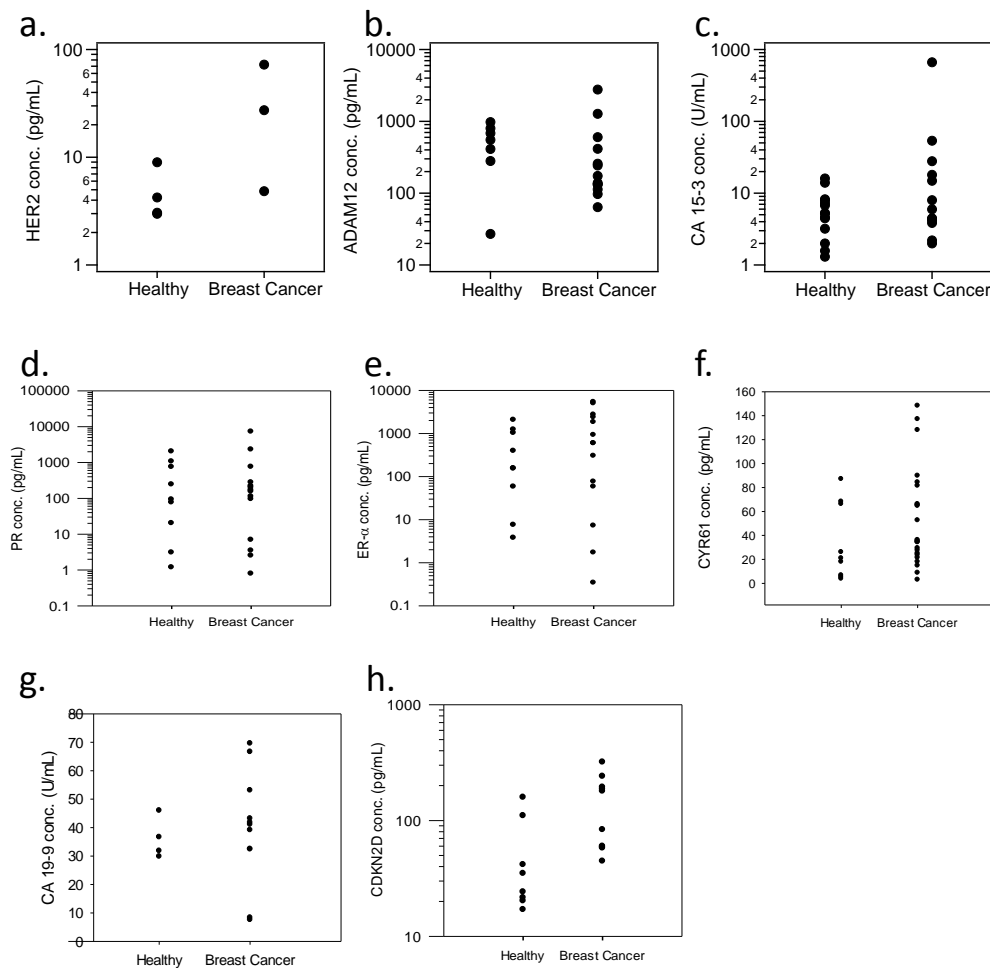
Figure 1. Results from screening healthy and breast cancer serum for: **a.** HER2, **b.** ADAM12, **c.** CA 15-3, **d.** PR, **e.** ER-α, **f**. CYR61, **g.** CA 19-9, and **h.** CDKN2D.
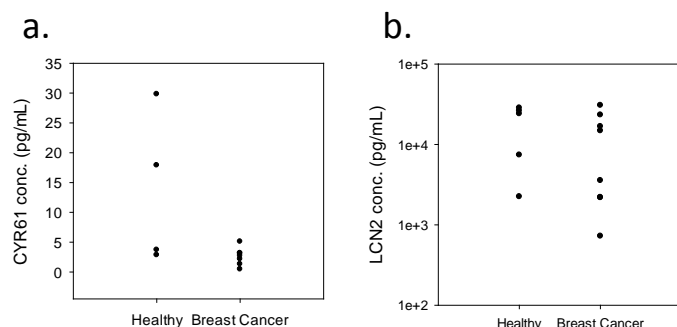
Figure 2. Urine screening results for **a.** CYR61 and **b.** LCN2in healthy controls and breast cancer patients.

2c. Expand sample set and run clinical samples with all assays developed for all markers (Year 5).
      These studies will be initiated with the expanded sample set provided by Dr. Buchsbaum.

2d. Determine which markers in blood correlate with disease using data processing and computational methods available in the laboratory (Year 5).
      These studies have not been initiated per SOW.

Task 3. Develop single cell analysis methods to determine composition of a primary tumor.

3a. Select approximately ten candidate markers (SNPs, proteins, etc.) of value for single breast cancer cell analysis in conjunction with collaborators (Months 1-9).
      We have chosen to utilize the pre-established PSA assay to validate SiMoA at the single cell level. This assay has proven to be extremely sensitive and our goal is to take advantage of the sensitivity of this established assay for single cell resolution.[11] In order to test this assay within cells, we have cultured the prostate cancer cell line LNCaP (cell lines were purchased from ATCC and donated by the Kuperwasser lab). We are also working towards developing single cell assays using the HER2 and PR SiMoA assays established in Task 1. Breast cancer cell lines T-47D and BT-474 will be used to quantify these markers in single cells.

3b. Detect presence of mtDNA by screening for many sequences using cultured cell lines and HIM tissue samples to select which markers to use. Will require development of mtDNA microarrays and sample screening (Months 6-18).
      The selection of mtDNA markers is being performed in conjunction with the Sonenshein laboratory (see Sonenshein Task 1 below). The DNA assay developed above in Task 2 will be the basis for the assays we plan to use for Tasks 3b and 3c.

***3c. Develop assays for the selected markers (Months 6-24).***
      The SiMoA assay for PSA has already been developed. PSA is being used as a proof of concept because it is well established. SiMoA assays for PR, ER-α, and HER2 have been developed as described in section 1. These markers will be useful for single cell studies of breast cancer cell lines such as T-47D and BT-474.

3d. Develop single cell assays for selected markers (Months 18-36).

We have spent considerable time developing a SiMoA single cell assay for detecting PSA in LNCaP cells as a proof-of-concept model since the PSA assay is well studied, reliable, and has a very low SiMoA detection limit (~0.01 pg/mL). Previously, all assays were carried out manually using optical fiber bundle arrays, which require several hours of hands-on preparation. Additionally, cells were previously isolated by diluting a stock cell suspension. However, this preparation is inconsistent and challenging to verify accurate cell counts. Using our previous protocols we could detect PSA levels down to 5 cells. To improve our assay for single cell resolution, we adapted our protocols for the automated HD-1 analyzer developed by Quanterix Corporation and collaborated with the Chiu lab to isolate and verify single cells.

The HD-1 analyzer fully automates all assay incubation, washing, and imaging steps, yielding consistent sample handling and maintaining ultrasensitive detection. Single cells were isolated by pipetting 1 µL cell suspension into PCR tube caps. The number of cells present in the droplet was confirmed under a microscope. Isolated cells were lysed in 64 µL lysis buffer, diluted in an additional 75 µL of sample diluent (total volume = 140 µL), and analyzed by HD-1.

Interestingly, we found that the LNCaP cell line purchased directly from ATCC exhibited significantly higher PSA expression than the cell line donated by the Kuperwasser lab. Cell line verification by short tandem repeat (STR) profiling indicated that the cell line donated by the Kupwasser lab had an 88% match to LNCaP. Cell lines with ≥80% match in their STR loci are considered to be related. Cancer cells are genetically unstable so it is expected that protein expression will change in highly cultured cell lines. The cell line donated by the Kuperwasser lab exhibited an average of 6.97 x10^4 PSA molecules/cell compared to an average of 2.06 x 10^6 PSA molecules/cell found in the LNCaP cell line obtained from ATCC. **Figure 3** shows the distribution of PSA molecules detected in single LNCaP cells from ATCC, which seem to fit well with a log-normal distribution.
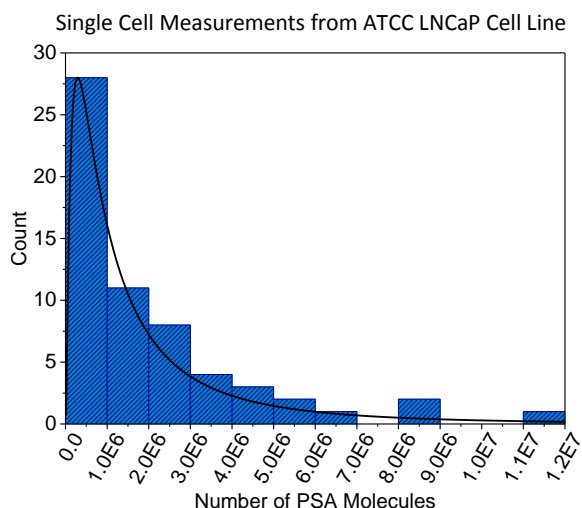
Figure 3. Histogram analysis of the number of PSA molecules detected in single LNCaP cells using SiMoA.

From this proof-of-concept study we have successfully quantified the number of target protein molecules in single cells for cell lines exhibiting both high and low protein expression. The success of

this technique will allow us to move forward with future single cell studies on breast cancer cell lines and eventually with tissue samples.

3e. Obtain tissue samples from HIM (Kuperwasser) and perform single cell analysis (Months 36-48).

These studies have not been initiated per SOW.

3f. Determine if one can observe rare cells with more aggressive genotypes or protein levels in HIM samples (Months 42-54).

These studies have not been initiated per SOW.

3g. Confirm presence of the single cells in human breast cancer biopsy samples obtained from Buchsbaum (Months 48-60).

These studies have not been initiated per SOW.

Daniel T. Chiu, PhD, *University of Washington, Seattle Campus Box 351700 Seattle, WA 98195-1700*

Task 1. Work with Walt lab to develop/refine single-molecule and single-cell techniques for analyzing protein and cell biomarkers (Months 1-36).

Task 1 will use cultured cell lines, commercially available serum samples, and serum samples from HIM model.

For Task 1, we have developed a new technology for the detection and analysis of cell biomarkers, in particular, circulating tumor cells (CTCs). CTCs have emerged as an important and valuable biomarker for the prognosis of breast cancer, and the sensitivity we have demonstrated makes CTCs a robust biomarker for prognosis and as an indicator of treatment efficacy. The high sensitivity also has the potential to make CTCs a diagnostic tool if they are present at sufficient levels in blood. Below, we describe each subtask in more detail.

1a. Develop microfluidic devices for sample preparation and optical manipulation. Initial devices will contain only sample preparation module for use by Walt lab (Years 1-2).

Last year, we reported on the successful completion of a CTC analysis method called ensemble-decision aliquot ranking, or eDAR, which combined the following components: multi-color line-confocal fluorescence detection with a high sensitivity, a hydrodynamic switching mechanism, a cell trapping and subsequent purification process, and an identification and downstream analysis sections. It had a high throughput, analyzing 1 mL of whole blood in 20 minutes, with over 90% recovery ratio and a zero false positive rate for spiked-in cultured cancer cells. The development of eDAR for CTC enumeration is essentially complete. The isolated CTCs may be further studied with single-cell techniques, such as single-cell digital PCR and digital ELISA.

1b. Integrate assays and optical methods developed in Walt lab into a microfluidic device for the analysis and profiling of biomarkers (Years 1-2).

A key step to integrate the single-molecule array technology developed in the Walt lab for the analysis of CTCs is to remove the CTCs from the sample preparation chip described above so that CTCs can be lysed and the important but low abundance protein biomarkers derived from the CTCs can be detected and quantified using the single-molecule array technology. Here, we have developed a simple workflow based on the manual handling of single cells, and have shown this approach works for the

digital PCR analysis of single cells (more details below). This manual method for preparing single-cell samples also works for digital ELISA, but the throughput needs further improvement.

1c. Develop integrated microfluidic and optical techniques for single cell analysis using model cell lines (Years 1-3).
    To address the throughput issue in 1b, we are developing an automated cell dispensing system for eDAR so that each isolated cell can be deposited into a well of a 96-well plate for high-throughput downstream single-cell digital analysis. Additionally, to facilitate the parallel manipulation of a large number of single cells, we have also explored the use of bipolar electrodes for the dielectrophoretic trapping and manipulation of single cells.

    Parallel manipulations of single cells with bipolar electrode (BPE) based dielectrophoresis (DEP). An ongoing challenge in single-cell analysis is manipulation (e.g. transport, sorting, trapping, and filtering) of the cells of interest. DEP manipulation of cells has been used to accomplish all of these functions while maintaining a high degree of cell viability. DEP is especially attractive for several reasons. First, cells can often be distinguished without the addition of labels (e.g. magnetic particles or fluorophores) owing to polarizabilities unique to cellular phenotype, size, and viability. Second, DEP devices are generally comprised of planar electrodes or insulating barriers made of sufficiently inexpensive components to allow the production of disposable devices, an especially desirable characteristic for diagnostic or prognostic devices, for which cross-contamination must be avoided. Third, DEP has been demonstrated to be useful for single cell manipulation. This has been accomplished by constraining the trapping point either by adding physical barriers or by defining an electric field cage similar in size to a single cell. In either case, DEP conditions are chosen that prevent cell-cell attraction, thus discouraging multi-cell capture. Finally, DEP can be more easily operated in parallel versus some competing technologies such as optical tweezers or purely fluidic systems, which require a network of pumps and valves.
    Despite these major advantages, current DEP technologies have remaining challenges to overcome, and three of the most serious shortcomings relate to the generation of the electric field gradient required for DEP force. First, while DEP technologies can be operated in parallel, there are practical barriers to achieving an array of local electric field gradients. There are two common ways of forming gradients in an applied electric field – namely, 1) by applying a non-uniform field with closely spaced electrodes and 2) by constraining the field with insulating barriers. Devices that form electric field gradients based on electrode arrays require the fabrication and actuation of many electrodes and wire leads – thereby leading to complex design and external instrumental control. Devices comprised of insulating barriers can only achieve precise trapping locations in positive DEP operating conditions, in which cells are trapped at vertices or constrictions where electric field maxima may be damaging to the cells.
   Second, the range over which DEP force exists around these electrodes and insulating barriers can be too short for high-throughput device operation. Specifically, significant field gradients are often effective over one to several cell diameters. This problem has been partially addressed by complex device fabrication techniques that implement 3D electrodes, including modification of microfluidic channel walls and ceiling.
    Third and finally, the shape of the electric field gradient produced by each of these strategies is fixed, lacking plasticity. One recently developed technology, optical DEP (or optoelectronic tweezers, OETs), has addressed this shortcoming through real-time light-based patterning of 'virtual electrodes' in a semiconducting layer under a DEP chamber. While OETs offer unprecedented spatial control over DEP force, the integration of OET materials and structures with existing microfluidic modalities is non-trivial.
   To address these shortcomings of current DEP for parallel single-cell manipulations, we employed BPEs to exert DEP force, and we modulate this force *via* the local conductivity of an aqueous medium. This technique differs from medium conductivity gradient DEP described above, used to sort and manipulate cells based on their conductivities, in that here, steeper gradients are locally and

electrochemically generated, thus enabling them to contribute significantly to the DEP force experienced by cells near the BPE. As a result, cells are trapped or repelled by the resulting electric field gradients. Importantly, this technology addresses each of the challenges faced by existing DEP technology. First, BPEs can be operated in an array format without requiring wire leads (electrical contact) to each individual BPE. As a result, the device is simple to fabricate. Second, the electric field gradients, which exert DEP force on the cells, have controllable size and can traverse the microchannel cross-section. This feature is important because the device dimensions and throughput are not limited by short-range DEP forces. Finally, the shape of the electric field gradient can be tuned fluidically. In the following sections we describe the operating principles of the DEP at a BPE and describe initial results demonstrating the manipulation of single cells.

Bipolar electrode (BPE). **Figure 4a** is an illustration of a BPE – here, a planar strip of conducting material – in a microfluidic channel. When a DC voltage bias is applied across the fluidic channel, a linear potential profile develops (solid line, **Figure 4b**). The potential of the BPE (U_{BPE}) floats to a value intermediate to the potential of the aqueous solution in contact with its ends. The potential difference (η) between the BPE and solution is a driving force for oxidation (η_a) and reduction (η_c) reactions at opposite ends of the BPE. Importantly, faradaic reactions are achieved at the BPE without direct electrical contact to the BPE, and this feature allows multiple BPEs to be operated in parallel. The rates of electron transfer to (oxidation) and from (reduction) the BPE are coupled and lead to a current through the BPE (i_{BPE}). Note that when i_{BPE} is non-zero, it competes with ionic current in the microchannel and impacts the potential drop in solution as indicated by the dashed line in **Fig 4b**.
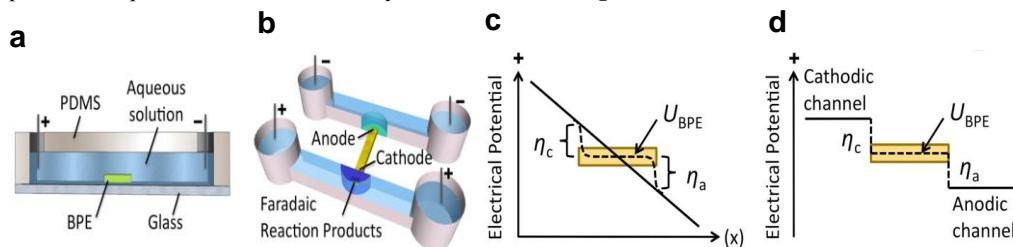
Figure 4. Microfluidic devices comprising a bipolar electrode and illustration of overpotential (η).
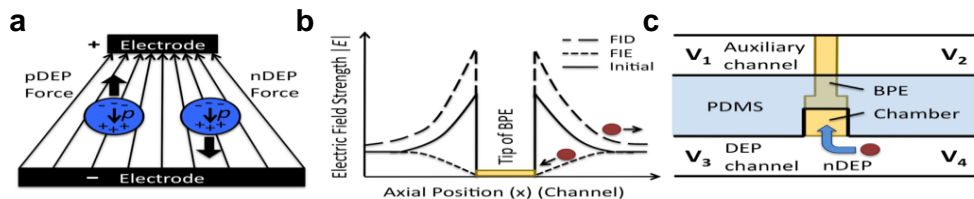
Figure 5. Principles of nDEP repulsion and capture at FID and FIE zones near a BPE tip

Generation of faradaic ion enrichment and depletion (FIE and FID) zones. Faradaic electrochemistry at the BPE ends can perturb the electric field through the formation of FIE (high conductivity, low field strength) or FID (low conductivity, high field strength) zones. For example, an increase in local ionic strength at the anodic end of a BPE has been demonstrated to occur *via* water oxidation followed by Tris buffer protonation. Within the confinement of a microfluidic channel, this increased concentration of TrisH$^+$ cations can remain localized around the anodic end of the BPE. Anions will electromigrate to charge pair with these cations, forming an FIE zone. Importantly, any oxidation or reduction reaction

adding charge to a solution-phase species can similarly lead to an accumulation of positively and negatively charged ions at *either* the BPE anode or cathode. Conversely, a decrease in local ionic strength at the cathodic end of a BPE has been demonstrated to occur *via* water reduction followed by Tris buffer deprotonation. The net result of this series of reactions is the neutralization of the buffer cation, TrisH$^+$ to neutral Tris. In this case, the co-anion (Cl$^-$) was shown to migrate away from the site of neutralization, thus leading to localized FID at the BPE cathode. Likewise, the neutralization of any charged species can lead to formation of an FID zone. Importantly, the shape and position of the FIE and FID zones can be controlled using convection.

Finally, these FIE and FID zones have been formed at BPE ends that are fluidically isolated as shown in **Figure 4c**. In this case, the solution potential in contact with the BPE in the cathodic channel is higher than U_{BPE} and in the anodic channel, is lower than U_{BPE} (**Figure 4d**). A key advantage of this device configuration is that the applied DC voltage required to drive faradaic processes is significantly lower than in the single channel design. This improvement is owed to the removal of an ionic current path (fluidic junction) between the anodic and cathodic driving electrodes.

DEP manipulation of cells using BPEs. We utilized these FIE and FID zones for DEP attraction and repulsion of biological cells. The mechanism by which ion concentration impacts DEP force is described here briefly. A polarizable particle subjected to an electric field will develop an induced dipole moment, p (**Figure 5a**). The magnitude of the dipole depends upon the volume of the particle, its degree of polarizability, and the strength of the surrounding electric field (E). In the presence of an electric field gradient, the particle will be attracted to regions of higher $|E|$ if the complex permittivity of the particle (ε^*_p) is greater than the complex permittivity of the surrounding medium (ε^*_m). This condition is called positive DEP (pDEP). Conversely, negative DEP (nDEP) will occur if ε^*_p is less than ε^*_m. The magnitude of DEP force (F_{DEP}) exerted on a spherical particle is given by: $F_{DEP} = 2\pi r^3 \varepsilon^*_m \text{Re}[K(\omega)] |E|^2$, where r is the particle radius and $\text{Re}[K(\omega)]$ is the real part of the Clausius-Mossotti factor (K), which is a function of electric field frequency (ω), because $K = (\varepsilon^*_p - \varepsilon^*_m)/(\varepsilon^*_p + 2\varepsilon^*_m)$ and $\varepsilon^* = \varepsilon + (i\sigma/\omega)$.

The above equations highlight the dramatic impact that a local change in solution conductivity (σ) can have on F_{DEP}. Specifically, the formation of an FID zone leads to an ohmic increase in the local magnitude of E, and simultaneously, causes ε^*_m to decrease (making K more positive). Likewise, FIE can have the opposite effect on E and ε^*_m. This synergistic effect is important because, as a particle is attracted (for instance, by pDEP into a high $|E|$ region), the magnitude of K can increase, leading to amplified attraction. These conductivity gradients act as extensions to the BPE, thus impacting a larger volume than the electric field gradients surrounding a typical planar electrode. **Figure 5b** (not to scale) illustrates the anticipated impact of FIE and FID on the axial component of the electric field adjacent to *either end* of a BPE in a microfluidic device (such as that depicted in **Figure 4c**). This simplified depiction assumes that the driving voltage applied to the device is symmetrical about the BPE. At an active BPE (ie. $i_{BPE} \neq 0$) the electric field is zero directly above the BPE and enhanced at the BPE edges (**Figure 5b**, solid line). The formation of an FIE zone leads to an ohmic decrease in the local magnitude of E, with the greatest impact nearest the BPE. At the BPE, the electric field remains to be zero. A cell will be trapped by nDEP at the resulting electric field minimum, at which the cell has a reduced risk of electric field-induced damage. Conversely, FID leads to an increase in the local magnitude of E, leading to enhanced and extended nDEP repulsion of a cell from the BPE. Previous measurements and simulations of E have shown that an electric field gradient formed by FIE and FID can extend up to several hundred microns from the BPE.

nDEP attraction of single cells to an FIE zone at the BPE anode and the BPE cathode. Here, we demonstrate nDEP attraction of single cells to the BPE with the addition of a DC offset. The DC field can drive faradaic current (i_{BPE}) leading to an FIE zone at either a BPE anode or a BPE cathode. Due to the negative charge of the cell membrane, in these two cases DEP force works with and against electrophoretic (EP) force, respectively. First, we will examine nDEP attraction of a B-cell to an FIE zone

at the *BPE anode* in Tris DEP buffer (**Figure 6a-c**). In this device, nDEP cell trapping proceeded at the BPE anode as follows. First, the flow was established such that v_{avg} = 65 μm/s. An AC field with a negative DC offset was applied at V_3 versus ground (V_1, V_2, and V_4) such that $E_{RMS,avg}$ = 5.7 kV/m AC and $E_{DC,avg}$ = 0.75 kV/m DC. **Figure 6a** shows the resulting cell trajectory in 1s slices. Under these conditions, the EP force exerted by the BPE anode was insufficient to attract and trap the B-cells. However, as the AC field strength was increased (**Figure 6a-6c**; $E_{RMS,avg}$ = 5.7 kV/m, 13.3 kV/m, and 17.7 kV/m, respectively) cells were increasingly attracted and finally trapped. This finding is significant because nDEP attraction toward the BPE indicates that the electric field is depressed around the BPE by FIE. At later timepoints than those displayed in **Figure 6c**, the trapped cell was pulled into the microchamber and remained over the BPE. This result is attributed to an averaged axial electric field profile like that shown in **Figure 5b** (dashed line indicating 'FIE'). Importantly, although E is zero above the BPE whenever i_{BPE} is non-zero (solid and dashed lines, **Figure 5b**), cells can only be attracted to this region after an FIE zone forms.

Likewise, we carried out nDEP trapping of a single cell at the BPE *cathode* (**Figure 6e-d**). In this case, a similar device was filled with 10 mM phosphate (pH 7.2) in 8% sucrose, 0.3% dextrose, and 0.1% BSA (phosphate DEP buffer). An AC field with a positive DC offset was applied at V_3 such that $E_{RMS,avg}$ = 5.7 kV/m AC and $E_{DC,avg}$ = 1.5 kV/m DC. Water reduction followed by deprotonation of phosphate species led to ion enrichment around the BPE tip. As the AC field strength was increased gradually from 5.7 kV/m to 28.3 kV/m, the cell was pulled into the chamber by nDEP (**Figure 6d**, 4 s/slice), and as the AC field was returned to 5.7 kV/m, the cell was expelled from the chamber (**Figure 6e**, 2 s/slice). This result is significant for two reasons. First, as in the previous experiment, this result demonstrates that faradaic current leading to FIE sufficiently decreases the local electric field around the BPE to reverse the role of nDEP from repulsion to attraction. Second, in this case, the cell was trapped by nDEP force despite electrostatic repulsion of the negatively charged cell from the BPE cathode. The role of EP is underscored by the immediate expulsion of the cell from the chamber once the AC field strength was decreased (**Figure 6e**). Importantly, this result has been repeated with the BPE misaligned from the chamber such that the two features are laterally separated by 50 μm and the BPE extends 15 μm into the channel (results not shown). In this control experiment, regardless of the direction of flow, cells favored trapping at the BPE rather than the chamber. This result verifies that the zero electric field directly above the BPE and FIE depression of the surrounding field are the primary mechanisms responsible for cell trapping. Furthermore, we performed a control with no BPE (results not shown). While the electric field in an empty chamber (no BPE) is lower than that in the microchannel, at AC field strengths up to E_{avg} = 28.3 kV/m, cells are only weakly attracted to the chamber and are only drawn into it under stopped-flow conditions.
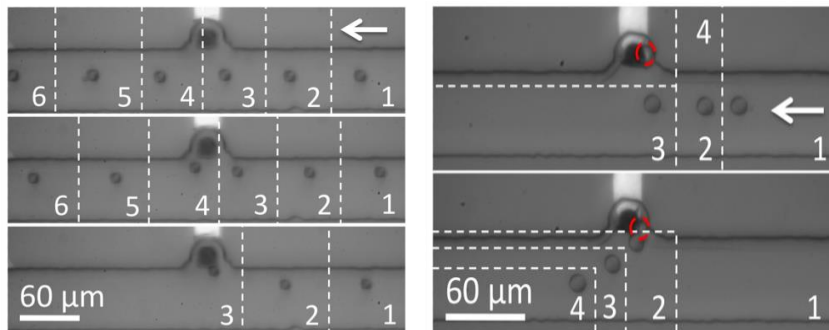
Figure 6. a-c) Multiple series of optical micrographs showing increasing nDEP attraction of a cell toward the BPE anode in Tris DEP buffer. $E_{DC,avg}$ = 0.75 kV/m, $E_{RMS,avg}$ for a) 5.7 kV/m, b) 13.3 kV/m, c) 17.7 kV/m. Image slices are 1 s apart. d) nDEP attraction of a B-cell toward the BPE cathode in phosphate DEP buffer (4 s/slice). $E_{DC,avg}$ = 1.5 kV/m, $E_{RMS,avg}$ increased from 5.7 kV/m to 28.3 kV/m from t = 0 s (slice 1) to t = 8 s (slice 3). e) Release of the trapped cell (2 s/slice) from (d) upon subsequent decrease of $E_{RMS,avg}$ to 5.7 kV/m (from slice 1 to slice 2).

Now that we have developed an in-depth understanding of BPE-DEP based single-cell transport and trapping, we are investigating several BPE array formats for array-based single-cell trapping and isolation. This technology will provide a powerful tool for parallel single-cell analysis after eDAR isolation of CTCs, which may offer the necessary throughput for downstream single-cell analysis using various digital formats, such as digital PCR and digital ELISA.

Task 2. Work with the Walt lab to apply these methods to breast-cancer patient samples for the detection and validation of protein and cell biomarkers *(Months 25-60).*

2a. Develop/submit amended proposal to University of Washington IRB to permit secondary use of currently archived patient samples (Months 1-12).
      This task has been completed per last year's annual report.

2b. Apply sensitive techniques (1a and 1b) for the retrospective analysis and validation of biomarkers from archived patient samples (Months 25-60).
      We propose to use archived blood plasma samples from breast cancer patients. One hundred archived blood plasma samples already exist in the Chiu lab from a previous three-year study on detection of biomarkers in breast cancer patients. Some of these samples have been analyzed by the Walt lab.

2c. Apply sensitive techniques (1a and 1b) for the prospective analysis and validation of biomarkers from patient samples (Months 36-60).
      We have started this task and have analyzed 11 patient samples thus far. The table below shows the results. We are at the early stage of analyzing this data.

Sample ID	Labeling Scheme	CTCs/ml	Subtype	Stage
B-140000007-1	1 step EpCAM	8	Triple -	Stage 4
B-140000053-1	1 step EpCAM	1.5	ER+, PR- Her2+	Stage 2
B-140000089-1	1 step EpCAM	0	ER/PR+ Her2-	Stage 2
B-140000122-1	1 step EpCAM	4	ER/PR - Her2+	Stage 4
B-140000169-1	Cocktail (EpCAM, HER2, EGFR, N-cadherin)	32	ER/PR+ Her2-	Stage 3
B-140000169-1	1 step EpCAM	8	ER/PR+ Her2-	Stage 3
B-140000477-1	Cocktail (EpCAM, HER2, EGFR, N-cadherin)	15	ER/PR + Her2 -	Stage 2
B-140000865-1	1 step	0	ER/PR- Her2-	Stage 4
B-140000931-1	1 step	29*	ER/PR+ Her2-	Stage 4
B-140001155-1	Cocktail (EpCAM, HER2, EGFR, N-cadherin)	27*	ER+PR-Her2-	Stage 1A (T1N0)
B-140001155-1	1 step	5*	ER+PR-Her2-	Stage 1A (T1N0)
B-140001165-1	1 step	4*	ER/PR+ Her2-	Stage 2
B-140001165-1	Cocktail (EpCAM, HER2, EGFR, N-cadherin)	0	ER/PR+ Her2-	Stage 2
B-140001241-1	1 step	0	ER/PR- Her2+	Stage 2
B-140001241-1	Cocktail (EpCAM, HER2, EGFR, N-cadherin)	0	ER/PR- Her2+	Stage 2

*These CTCs also expressed CD45

Based on the above clinical studies, we found CTCs isolated from patients to be highly heterogeneous, both in terms of the amount of cell-surface proteins that the CTCs express and the types of cell surface proteins present on the CTCs. As a result, we carried out a systematic study to determine the minimum number of proteins needed on CTCs in order for eDAR to capture them efficiently. We further improved the ability of eDAR to capture CTCs with low levels of expressed proteins by developing a cocktail of antibodies to label multiple proteins on CTCs. We are also developing brighter probes to tag the low expression proteins so they can be better detected by eDAR.

Limit of detection (LOD) of eDAR and strategies for increasing the number of CTCs isolated from patients. To understand the LOD of eDAR, we first characterized the brightness of the different breast cancer cell lines known to express various amounts of the cell surface protein EpCAM (currently the cell surface marker used for isolation of CTCs) and then determined the number of EpCAMs present on each cell based on the number of fluorescent antibodies bound to EpCAM. To quantify the number of

fluorescently bound antibodies, we calibrated eDAR using fluorescent beads commonly used to calibrate and determine the number of fluorophores bound to cells in flow cytometry. **Figure 7** shows the calibration results; there is a strong correlation between the brightness in eDAR and flow cytometry. To calculate the LOD for eDAR, we used a labeled blood sample without cells and found the standard deviation (σ) of the background, and LOD is just 3σ. For robust eDAR sorting of single CTCs, often we require a higher S/N (signal to noise) than LOD. Specifically, we often require a S/N of 10; we call this higher S/N of 10 the limit of quantitation (LOQ). We determined our current eDAR LOD is 5800 EpCAMs and LOQ is 23500 EpCAMs per cell.
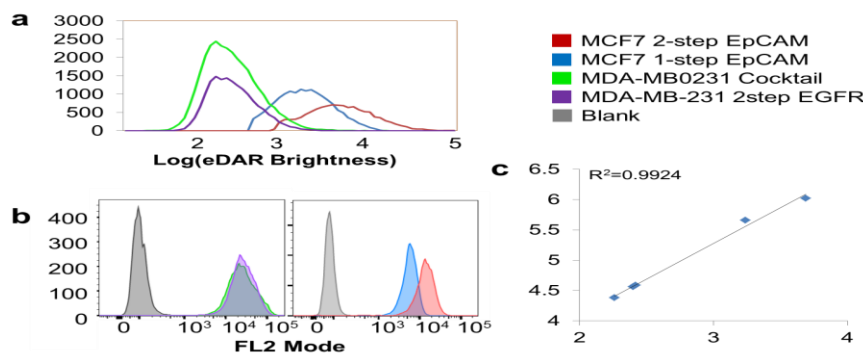
Figure 7. a) eDAR brightness from the four cell populations used in the calibration, graphed on a log scale. b) Flow cytometry histograms of the same four populations. c) Plot of brightness in eDAR (x axis) vs brightness observed in flow cytometry (y axis), showing excellent correlation.

CTCs with low protein expression are generally categorized as those with less than 10,000 molecules/cell. While our LOD is below this level, our LOQ is above this threshold. To address this issue, we tried to increase our LOQ by using a two step labeling protocol; at present, we use fluorescently labeled primary antibodies, but the use of fluorescently labeled secondary antibodies may amplify our signal two fold because of multiple binding of secondary antibodies to the primary. Additionally, we tried to use a cocktail of antibodies against multiple cell surface proteins, and in this case, the use of fluorescently labeled secondary antibodies also provide practical advantages because they can label all primary antibodies bound to the cell surface. This way, the relative amount of fluorescent antibodies present on the cell surface is additive without also seeing an additive increase in the background signal as would happen with fluorescently conjugated primary antibodies.

To demonstrate this improvement, we spiked in cultured cells into clinical samples from breast cancer patients. Here, we used MDA-MB-231 cells, both because they are models for triple negative breast cancer and because they are considered low to negative for EpCAM expression. **Figure 8** illustrates the improvement seen from using a primary anti-EpCAM antibody (1 step), a fluorescent secondary antibody (2 step), and a cocktail of primary antibodies labeled with the same fluorescent secondary antibody. The primary antibodies used in the cocktail were against EpCAM, HER2, EGFR, and N-caderein. EpCAM is an epithelial surface markers that have been reported in CTCs; HER2 was used for marking potential HER2$^+$ breast cancer cells; EGFR and N-cadherin is a mesenchymal marker that has been noted in the EMT of CTCs, so it was added to the cocktail in the hopes of detecting CTCs that have undergone EMT.
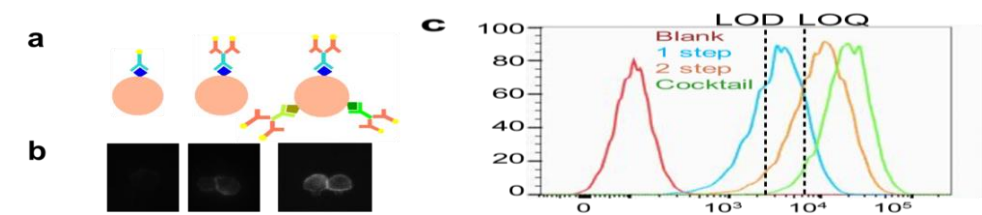
Figure 8. a) Schematic of the three labeling strategies we used: 1-step EpCAM, 2-step EpCAM, 2-step cocktail. b) Images of MDA-MB-231 cells labeled with each of the three strategies. c) Flow cytometry histogram of the three strategies, showing where the LOD and LOQ fall.

Figure 8 shows the majority of PE-anti-EpCAM labeled MDA-MB-231 cells cannot be isolated by eDAR; the use of fluorescently labeled secondary antibodies to amplify the signal helped, but still insufficient for isolating the majority of MDA cells by eDAR. But for MDA cells labeled with the cocktail of antibodies, 86% are above the LOQ and thus can be isolated by eDAR. The markers chosen represent the expected and often described diversity among CTCs, such that it is expected that we would see more CTCs in patient samples using this method than with traditional EpCAM labeling. To test this hypothesis, we ran the same blood sample from a breast cancer patient twice, first using only fluorescently labeled primary against EpCAM and then with the cocktail strategy. This sample came from a stage 3 breast cancer patient, whose tumor was ER+, PR+, HER-. With only primary anti-EpCAM labeling, 8 CTCs/ ml were detected. But with the cocktail strategy, we isolated 32 CTCs/ml. **Figure 9** shows some example cells isolated from this patient. This result shows the importance of calibrating and understanding the LOD and LOQ of eDAR for CTC isolation, and lays the ground work for us to further improve the CTC labeling strategies so we can isolate more CTCs and also more diverse populations of CTCs from breast cancer patients, given the highly heterogeneous nature of these deadly cells.
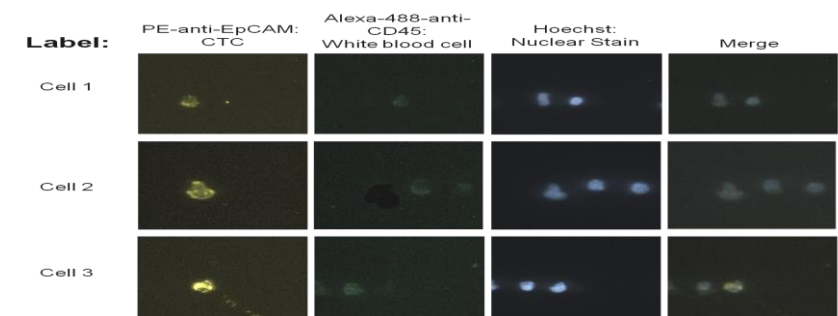
Figure 9. Three cells isolated from stage 3 breast cancer patient, whose tumor was ER^+, PR^+, HER^-.

Because of the highly heterogeneous nature of CTCs from patient samples, we have further developed an eDAR chip capable of simultaneous isolation and capture of different subpopulations of CTCs. We describe this development below.

Simultaneous and selective isolation of multiple subpopulations of CTCs from peripheral blood using eDAR. CTCs are physically and biologically heterogeneous. This heterogeneity is being increasingly recognized as an important issue in the isolation and analysis of CTCs, because simply relying on one set of markers or properties, either biological or physical, may undercount the number of cells and result in the loss of important subpopulations. For example, CTCs can exhibit highly variable

amounts of epithelial and mesenchymal markers because many of them may undergo the epithelial-to-mesenchymal transition (EMT), which is thought to play an important role in cancer metastasis. Furthermore, EMT markers on CTCs occur more frequently in metastatic than in early stage breast cancer and correlate more accurately with tumor progression than the expression of epithelial markers alone.

To address this need to study multiple subpopulations of CTCs, we re-designed the eDAR platform so that different subpopulations of cells can be simultaneously and selectively isolated from peripheral blood. In this "dual-capture" version of eDAR, a blood sample was first labeled with antibodies directed against two sets of biomarkers. Each type of antibody was conjugated with a different fluorophore. The labeled sample was then introduced into the microfluidic chip, divided into millions of virtual aliquots, ranked by a line-confocal detection scheme, and then selectively isolated and physically separated into two different areas of the microfluidic chip based on the expression level of the two markers. The recovery rate of each subset was higher than 88% without sacrificing eDAR's high throughput.

Because we aimed to simultaneously select two subsets of rare cells from whole blood, we labeled the blood sample with two types of fluorescent antibodies. **Figure 10a** summarizes the labeling procedure, which was optimized to minimize potential loss of sample and stress on the cells. If the two target subsets were CTCs with a high expression of EpCAM and CTCs with a low or even no expression of EpCAM because of EMT, then we labeled the blood sample with anti-EpCAM-Alexa 488 (green emission) and anti-EGFR-phycoerythrin (PE) (yellow emission). EpCAM has been widely used to capture epithelial CTCs; EGFR was used to isolate cells with a low expression of EpCAM and which may have acquired mesenchymal characteristics. Other mesenchymal markers, such as N-cadherin, can also be used to select the EpCAM^{low} CTCs.
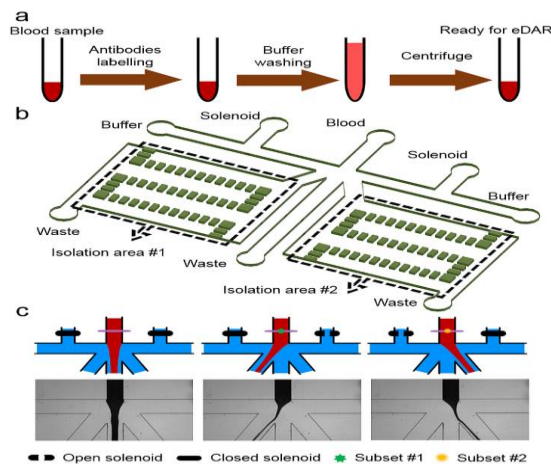

Figure 10. Schematic and images showing the working principle of dual-capture eDAR. (a) The general workflow of the immunostaining of a blood sample before eDAR. (b) Schematic of the dual-capture eDAR microchip; the green blocks are the microslits (5 μm gap) used to trap and retain CTCs while allowing all of the red blood cells and most of the white blood cells to pass through. (c) The active sorting mechanism for sorting the aliquots into 3 different channels; negative aliquots were sorted to the center waste channel, while aliquots having the two subpopulations of rare cells were sorted into the two different isolation areas.

After immunostaining, we introduced the labeled sample into the microfluidic chip at the flow rate of 50 μL/min. Figure 10b shows the design of the microchip used for dual-capture eDAR. Blood entered the center top channel and the two CTC subpopulations were then selectively enriched in the two isolation areas. The other channels were used to control the active sorting step, which is based on flow

displacement, or to remove waste. When the aliquots flowed across the laser beam, the line-confocal detection region (see the thin line with green and orange dot in **Fig 10c**) scanned each aliquot to determine if there were any CTCs stained with fluorescent antibodies. The aliquots were thus ranked into three groups, those with no CTCs, those that were positive to the first subset of CTCs, and those positive for the second subset. eDAR is flexible in applying complex logical decisions to the selection of rare cells. For example, to separate a subset from the population of epithelial CTCs, such as Her2$^+$ CTCs, we can apply the "AND" logic. We stained the blood with anti-EpCAM and anti-Her2, so any aliquot having a two-color signal was sent to the Her2$^+$ group. Similarly, we can include the "NOT" logic in the selection scheme to isolate a particular subset of rare cells without losing other rare cells using the dual-capture eDAR approach. This eDAR feature may be especially useful for the isolation of circulating breast cancer stem cells in the presence of regular CTCs because cancer stem cells are often defined by a combination of positive and negative control markers, such as CD44$^+$/CD24$^-$ for breast cancer.

To simultaneously and selectively isolate two subpopulations of rare cells, we re-designed the active sorting scheme of the eDAR approach. The flow-displacement switching scheme was similar to our previous work with important modifications (**Fig 10c**). When the aliquots were ranked as "negative", indicating the absence of rare cells, both solenoids were closed and the blood flow was focused into the center waste-collection channel by the two side buffer channels, which were constantly open to the pressurized buffer source. When the aliquot displayed a signal in the green fluorescence channel (EpCAM-Alexa488), the solenoid on the right side was opened, and the blood flow was pushed to the collection channel on the left. Similarly, an aliquot containing a CTC labeled with anti-EGFR-PE (yellow emission) was sorted into the collection channel on the right (**Fig 10c**).

The fluid switching time of the active sorting step is a key parameter that determines the performance of eDAR. Using a high-speed camera, we characterized the switching time of the following four steps: the switching time from center to left channel, the switching back from the left to center channel, the switching over from center to right channel, and the switching back from the right to center channel. From the high-speed images (**Fig 11a & 11b**), we determined the switch over time from the center to the left or right channel was less than 2 ms, and the switch back time from the left or right to center channel was less than 4 ms. Next, we tested the sorting efficiency using green and red fluorescent beads spiked into whole blood. We performed dual-capture eDAR for those samples until 1000 total green and/or red events were detected by the line-confocal detection system. The flow rate we used was 50 µL/min, and the sorted beads were collected in the two trapping areas and then enumerated visually with epi-fluorescence imaging (**Fig 11c**). For the first sample where we spiked in only green beads, we had about 95% of the beads trapped in the targeted area (isolation area #1), and did not observe any green beads trapped in the other isolation area (isolation area #2). Similarly, for the second sample with only red beads, the sorting efficiency was about 93%. In the third sample with mixed green and red beads, we had a sorting efficiency for green and red beads of 93% and 94%, respectively. This sorting efficiency of the dual-capture eDAR is similar to that of the regular eDAR.
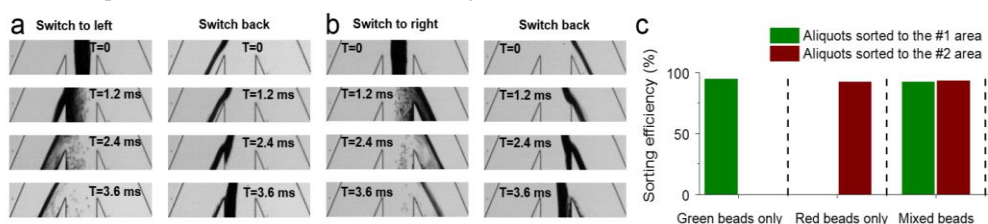
Figure 11. Hydrodynamic flow switching for the active sorting scheme. (a) Images taken with a high-speed camera showing the blood flow when the aliquot was sorted to the #1 isolation area on the left side. (b) Images showing the blood flow when the aliquot was sorted to the #2 isolation area on the right side. (c) Sorting efficiency measured with spiked-in fluorescent beads (green & red emission) at a flow rate of 50 µL/min.

As a model system, we spiked MCF-7 (high EpCAM expression; no/low mesenchymal characteristics) and MDA-MB-231 (low EpCAM expression; high mesenchymal characteristics) cells into healthy donor's blood, and then performed dual-capture eDAR experiments. After the two subpopulations of spiked-in cancer cells were sorted into the two different regions on the microchip, we removed all the red blood cells and some of the white blood cells from whole blood via on-chip filtration so the targeted rare cells could be trapped and imaged in the same microchip. We designed two separate filtration areas using a series of microslits (**Fig 10b**). To identify the captured cancer cells, we further stained them with antibodies conjugated with differently colored fluorophores against different biomakers on the cells. Because the two subsets of rare cells were in two separated isolation areas, we applied different sets of biomarkers that were specific for the targeted subpopulation. **Figure 12a** shows the two MCF-7 cells trapped in the isolation area #1 on one side of the chip (**Fig 10b**). EpCAM receptors on these cells were stained before the dual-capture eDAR experiment. After isolation by eDAR, we labeled this cancer cell subpopulation with additional biomarkers used to identify epithelial CTCs: cytokeratin, CD45, and Hoechst. The results clearly show these two cells were MCF-7, and not MDA-MB-231 cells. Similarly, we applied a different set of biomarkers for the other subpopulation of cancer cells trapped on the right side of the chip in isolation area #2: vimentin, CD45, and Hoechst. Figure 9b shows that the two cells trapped in isolation area #2 were positive for EGFR, vimentin, and Hoechst, consistent with the characteristics of MDA-MB-231 cells.

To evaluate the performance of the dual-capture eDAR, we spiked 25, 50, and 100 MCF-7 cells and the same number of MDA-MB-231 cells into 1 mL of healthy donor blood. After dual-capture eDAR, we enumerated the captured cells in the two purification areas based on the results of secondary labeling as described above. The average recovery efficiency for MCF-7 cells was 93%, and for MDA-MB-231 cells was 88%.

As dual-capture eDAR simultaneously isolates two subsets of rare cells into two different regions of the microchip, the method's selectivity is another important factor. To test this, we spiked 2000 MCF-7 and 2000 MDA-MB-231 cells into the same blood sample, performed dual-capture eDAR, and then imaged the cells after applying the same two sets of biomarkers described above: EpCAM/ cytokeratin/ Hoechst, and EGFR/ vimentin/ Hoechst. We did not find any targeted cells isolated in the area that was not designed for that particular subset.

The flexibility of using different criteria for the selection of rare cells by eDAR makes it possible to easily design devices for other applications. For example, Her2 is an important biomarker and a drug target for breast cancer patients so the isolation of CTCs that overexpress Her2 is useful. As a model system, we spiked MCF-7 (with low Her2 expression) and SKBr-3 (with high Her2 expression) into the same blood sample, and performed dual-capture eDAR. Because SKBr-3 cells also express EpCAM, we defined the high Her2 group based on the expression of both Her2 and EpCAM, and the low Her2 group based on being EpCAM positive but Her2 negative. The recovery efficiency for the Her2$^+$ subset of breast cancer cells was 92% and that for Her2$^-$ group was 94%. Other applications, such as the simultaneous isolation of CTCs and cancer stem cells from the same blood sample, also can be easily achieved with dual-capture eDAR. Moreover, we are able to capture other types of rare cells in addition to CTCs. For example, one potential application is the isolation and enrichment of CTCs and rare immune cells from the same blood sample in the same microchip so that the relationship between CTCs and rare immune cells can be studied.
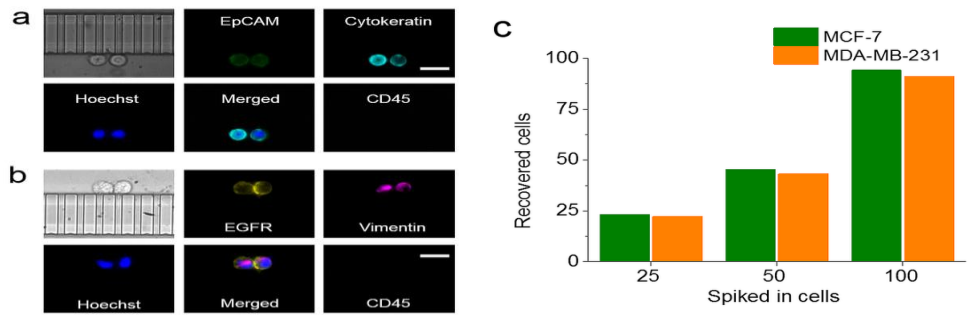
Figure 12. Simultaneous and selective isolation of EpCAM positive breast cancer cells and EpCAM⁻/EGFR⁺ breast cancer cells with the dual-capture microchip. (a) Two MCF-7 cells were trapped in isolation area #1 and stained with EpCAM, Cytokeratin, CD45, and Hoechst. (b) Two MDA-MB-231 cells were trapped in the isolation area #2 and stained with EGFR, vimentin, CD45, and Hoechst. The scale bars represent 25 μm. (C) The recovery efficiencies of MCF-7 and MDA-MB231 cells spiked in healthy donors' blood

In summary, we developed a new version of eDAR with a re-designed high-speed active sorting scheme so we could simultaneously isolate and enrich two subpopulations of CTCs from the same blood sample. The two subsets of rare cells were trapped in two separated areas on the microchip and then immunostained with different sets of biomarkers specifically designed for those two subpopulations. We demonstrated the simultaneous isolation of EpCAM⁺ breast cancer cells and EGFR⁺/EpCAM⁻ breast cancer cells, as well as the isolation of EpCAM⁺/Her2⁺ breast cancer cells and EpCAM⁺/Her2⁻ breast cancer cells. The recovery efficiencies of those subpopulations were higher than 88% with the selectivity close to 100%. This new capability should provide unique features in analyzing subpopulations of CTCs from breast cancer patients.

2d. Apply techniques developed for the prospective analysis of cancer cells (1a and 1c) from patient samples obtained in 2c with single-cell resolution (Months 36-60).

For the analysis of the CTCs with single-cell resolution, we have adapted a digital PCR (dPCR) platform that we had previously developed, called SD (self digitization) chip, for the genetic analysis of individual CTCs. We describe this single-cell dPCR technique below.

   Digital PCR (dPCR) assay of single cancer cells. Studying mRNA expression at the single-cell level can provide a means to characterize variability in cellular activity and thus study cancer etiology and pathology. Standard macroscale methods for quantitative assessment of gene expression are not designed to handle very small volumes and are limited by their sensitivity and accuracy when applied to single-cell analyses. In response to these challenges, we developed a technique that can carry out single-cell RNA-to-cDNA conversion in the same volume as the PCR reaction to quantify mRNA. Here, both reverse transcription and PCR occur in digitized volumes without prior reverse-transcription or pre-amplification, which are known to introduce copy-number bias. This is the first study to perform one-step digital RT-PCR for a single cell.
   Figure 13 shows an image and diagram of the device. To fill the device, we found that thermal stable oil-surfactant systems adopted from emulsion PCR systems ensure that the high temperatures achieved during thermal cycling do not cause digitized volumes to enter into the main channel where they might combine with neighboring volumes. Additionally, loading the chip with negative pressure, using a vacuum pump on the outlet *versus* positive pressure on the inlet, prevented overloading of individual

chambers in the compressible PDMS substrate. With these modifications, 88.0 percent (SD = 3.3%) of the single-cell sample was digitized in the 12 single cell experiments. In contrast, workflows for high-throughput, single-cell, microfluidic qPCR using preamplification of cDNA before digitization typically use less than 5% of the sample. Workflows not incorporating preamplification for single-cell assays, instead performing microfluidic digital PCR of cDNA, often digitize approximately 50% of the sample.
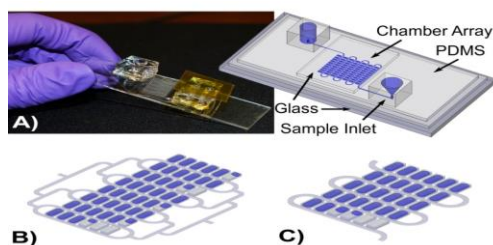
Figure 13. Components of the digital RT-PCR self-digitization chip. A) Image of assembled device with sketch of chip components. B-C) Possible chip designs include: B) Bifurcated chip design C) Serpentine chip design to minimize sample loss.
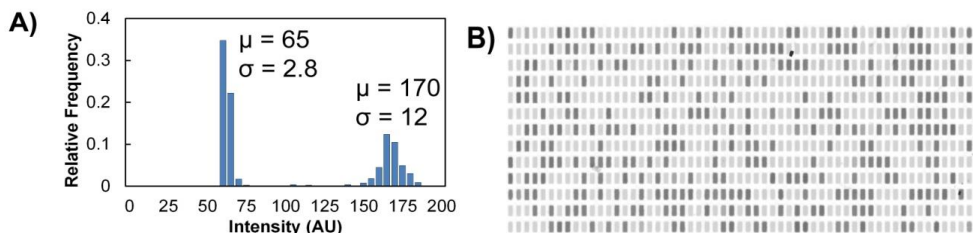

Figure 14. Post-amplification well intensity. A) Typical well intensity distribution for single-cell amplification of TFRC RNA. High intensity value indicates target amplification. B) Background-subtracted image of a serpentine array after single-cell digital RT-PCR. Dark volumes indicate target amplification.

Analysis of post-amplification array images showed two distinct intensity clusters for sample volumes corresponding to PCR-negative and PCR-positive reactions (**Figure 14**). From the proportion of positive to total volumes in the array, application of Poisson statistics allowed us to determine the concentration of molecules on the device. The Wilson score method was then used to calculate the 95 percent confidence intervals about this estimation.

The choice of enzyme to perform reverse transcription of RNA to cDNA was essential to assay performance. Ideally, each chamber in the array containing RNA would contain one or more corresponding cDNA molecule after reverse transcription, so that these chambers would yield a positive signal following PCR. For this reason, we chose a reverse transcription enzyme known for high-yield and stability. A long incubation time was used to allow the enzyme sufficient time for reverse transcription.

We first tested the ability of this device to perform digital and one-step RT-PCR by analyzing a dilution series of total RNA for glyceraldehyde-3-phosphate dehydrogenase (GAPDH) mRNA copy number. Response was linear (R^2 = 0.999) and matched closely to qPCR using a standard curve of

GAPDH RNA. The SD Chip indicated slightly lower quantities of GAPDH mRNA in the sample (qPCR 102 GAPDH copies per pg Total RNA, digital one-step RT-PCR 71.8 GAPDH copies per pg Total RNA) (**Figure 15A**). Errors inherent to real-time PCR calibration curves likely contributed to this variance, including UV absorbance measurements and variation in enzymatic reaction efficiencies between standards and total RNA samples. This finding is consistent with other studies comparing digital PCR and real-time PCR measurements.
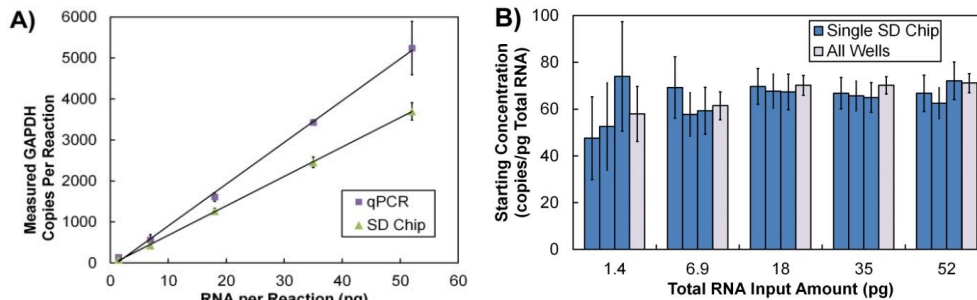

Figure 15. Amplification of GAPDH transcripts from total RNA. A) Measured GAPDH copies versus total RNA input measured by qPCR or the SD Chip. B) Estimated GAPDH starting concentration determined by digital RT-PCR at five dilution points. Dark blue bars represent concentration estimation and 95% confidence intervals (CI) for each run; light grey bars represent concentration and CI estimation for the sum of positive and total chambers for the three SD Chips analyzed at each dilution.

Results from the GAPDH mRNA dilution series were also multiplied by their dilution factors to return to the starting concentration of GAPDH mRNA in the total RNA starting sample (**Figure 15B**). The final two points in this dilution series fell slightly below the average starting concentration. This may be due to an error in the creation of the dilution series, either caused by pipetting error or a loss of the minute quantities of RNA inside pipet tips or vessels used to prepare reagents. These data are significant because it shows that any bias between low and high copy numbers of the mRNA transcript is minimal. However, this result does not show that the absolute quantities determined from the analysis reflect the absolute quantities of mRNA present in a single cell.

Having shown that the SD chip's digital one-step RT-PCR gave results comparable to the qRT-PCR, we next sought to validate the absolute quantification of mRNA in single cells by comparison with another single-cell mRNA quantification technique, single-molecule mRNA FISH. FISH is independent of the variable efficiency of reverse transcription and PCR and was developed specifically for quantification in single-cells. For these reasons, it is an excellent independent validation method. In this method, direct counting of single RNA molecules is performed in a sample of fixed cells by attaching multiple probes labeled with fluorophores along the length of each RNA molecule. With high-resolution fluorescence microscopy, it is possible to identify single RNAs as diffraction-limited spots in a z-stack of images. Challenges with probe design and spatial resolution of fluorescent signals limits the compatibility of this method for highly concentrated transcripts or for those that cluster within the cell. We chose to study the transferrin receptor (TFRC) gene, a relevant protein in cancer. The typical intercellular mRNA spatial distribution and concentration for this gene made it an excellent candidate for this study.

We found that results from both methods agreed well, yielding on average 455 ± 171 (n=31) copies of TFRC transcripts per single cell using FISH and 442 ± 207 (n=12) copies using the SD Chip with digital RT-PCR (**Figure 16**). This value is similar to TFRC values found in HeLa cells using single-molecule FISH. We also found that the distribution of TFRC mRNA copy number was similar between the two methods. The statistical error for dRT-PCR data, displayed as 95% confidence intervals, are small compared to the variation in TFRC in these cells. The magnitude of associated theoretical uncertainty per

cell in digital PCR is dependent on the total number of volumes analyzed, and thus can be reduced to fit the needs of the user by adding more reaction volumes per sample. Importantly, unlike single-molecule FISH, digital, one-step RT-PCR is not limited by the optical resolution of mRNA transcripts that cluster *in vivo*. The number of digitized volumes per device also can be scaled to quantify transcripts of any abundance.
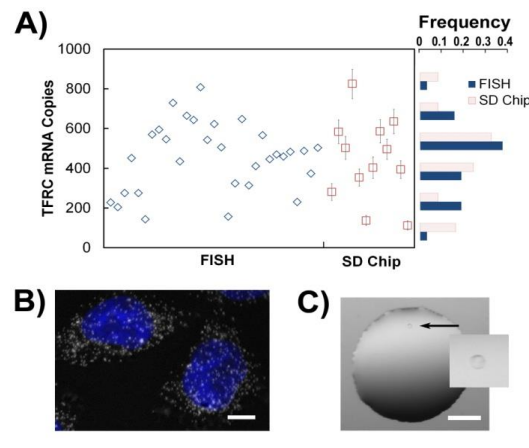
Figure 16. Absolute quantification of TFRC mRNA copies in single cells. A) Comparison of single-cell TFRC copy number distributions using FISH or the SD Chip. Individual single-cell measurements are presented (left) as well as the distribution of mRNA values (right). Histogram bin size is 150 mRNA copies. Average copy number, standard deviation, and distribution were similar for the two methods. B) False-color mRNA FISH image. Nuclei are colored blue and the TFRC mRNA appears as white spots. The scale bar is 10μm. C) Droplet containing a single cell in PBS to be used for analysis in SD Chip; the inset shows the single cell pointed to by the arrow. Scale bars are 100 μm.

The SD chip is a simple device for sample digitization that is compatible with single-cell digital RT-PCR. The device maximizes the fraction of sample digitized into the array, making the design ideal for working with the occasional low mRNA copy numbers present in a single CTC. We have demonstrated that digital RT-PCR with reverse transcription performed in the digitized volumes gives a linear response to the mRNA template concentration. Additionally, absolute quantification of mRNA from single cells agrees well with the copy numbers obtained from another absolute mRNA counting technique with the same transcript and cell line. Counting absolute quantities of mRNA allows us to overcome the need for a reference gene or calibration standard, which are restrictions at odds with the stochastic nature of gene expression at the single-cell level and introduce technical variability. Further improvements of the SD Chip for single-cell genetic analysis will focus on increasing throughput, for example, a multiple-channel parallel scheme for the rapid analysis of many cells.

Charlotte Kuperwasser, PhD, Tufts University School of Medicine, 750 Washington St., Box 5609 Boston, MA 02111

Task 1 Early Detection (Months 1 to 36)

1a. Utilize the 'Human-In-Mouse' breast tumor model to determine if one can identify biomarkers of early tumor progression and tumor growth. Collect blood and breast tissues at various stages of progression: Normal, hyperplasia, DCIS, invasive cancer (Months 1-18). HIM tumors will be created from human breast epithelial cells collected from discarded tissues of women who have undergone reduction mammoplasty surgeries. For more information/details on model: *Nature Protocols*, **2006**, 1, 595-599.

As described in last year's report, the goal of our studies for this year was to determine whether we could detect a known human biomarker in mouse serum using SiMoA technology and if so, use this biomarker to track the progression of tumor formation. Given the challenges we reported last year surrounding a positive control for human breast cancer, we instead decided to use prostate surface antigen (PSA), a known biomarker for prostate cancer as a proof of principle. Accordingly, we established several xenograft models using the human prostate LNCaP cell line. LNCaP cells are an epithelial cell line that originated from a metastatic lesion of a human prostatic adenocarcinoma and are commonly used in prostate cancer research.

This past year, we established 3 models to determine the lowest threshold of PSA detection in mice. To do this, we generated 62 LnCAP xenografts (a PSA+ model) for the Walt laboratory and provided mouse serum for analysis. Three different experiments were conducted.
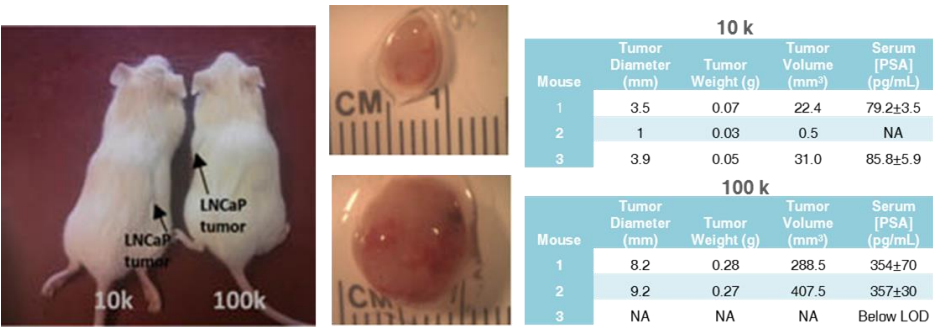
1) We injected mice with $3x10^6$ or $1.5x10^6$ cells and allowed for mice to develop tumors. This experiment determined whether PSA could even be detected in serum of PSA+ tumor bearing mice.

2) We implanted mice with 10^6 LnCAP cells and provided serum from these animals taken every day for 3 weeks. This experiment determined when during tumor formation with a large inoculum, PSA could be detected.

3) We inoculated mice with 10,000 cells or with 100,000 cells and provided serum from these animals taken every 3 days for 2 weeks to determine when during tumor formation PSA levels could be detected over time when very few cells were implanted into mice. This latter experiment established the lowest threshold of detection prior to the formation of tumors.

All three of these experiments have been completed and the serum analyzed by the Walt lab. **Figures 17 & 18** show representative tumors images, histology, and tumor formation data that were collected and included in a manuscript of this work. Results from these experiments were reported by the Walt lab in the July quarterly report. Briefly, PSA could be detected in the serum of mice collected 8 weeks following injection of $1.5X10^6$ cells that harbored large tumors (>8mm diameter) as well as mice that did not form tumors (<5mm) indicating that biomarkers could in fact be detected in the serum of mice 8 weeks after a large number of tumor cells were implanted.

In addition, an increase in PSA concentration in the serum of mice could be observed over time, the concentration of PSA in the serum of the majority of mice was indeed measurable at values well above the SiMoA detection limit. All values measured with SiMoA prior to tumor formation were below or at the detection limit of commercially available ELISA kits. Two out of three mice developed large tumors (>8 mm in diameter) after eight weeks and had significantly elevated serum PSA levels (355±2 pg/mL) compared to the rest of the mice. Notably, the mouse that did not develop a tumor after eight weeks also

had undetectable levels of PSA. The mice with tumors were the only samples with serum PSA concentrations that would have been easily detected using standard ELISA.

The sensitivity limits of SiMoA were also established with our mouse model. Indeed, an increase in PSA concentration was observed over time, with a large increase where palpable tumor formation occurred. Thus, these studies have established 1) a human biomarker can indeed be measured in the serum of mice using SiMoA, 2) SiMoA is highly sensitive and can successfully detected ultra-low levels of a biomarker in occult tumors in mice and 3) SiMoA can successfully follow and measure tumor formation even PRIOR to frank palpable tumor development.

10 k

Mouse	Tumor Diameter (mm)	Tumor Weight (g)	Tumor Volume (mm³)	Serum [PSA] (pg/mL)
1	3.5	0.07	22.4	79.2±3.5
2	1	0.03	0.5	NA
3	3.9	0.05	31.0	85.8±5.9

100 k

Mouse	Tumor Diameter (mm)	Tumor Weight (g)	Tumor Volume (mm³)	Serum [PSA] (pg/mL)
1	8.2	0.28	288.5	354±70
2	9.2	0.27	407.5	357±30
3	NA	NA	NA	Below LOD

Figure 17. LnCAP xenografts. Representative images of small subcutaneous xenograft tumors growing in NOD/SCID mice when inoculated with 10,000 or 100,00 cells. Representative brightfield images of xenograft tumors and sizes. Tumor formation summary tables and PSA detection.
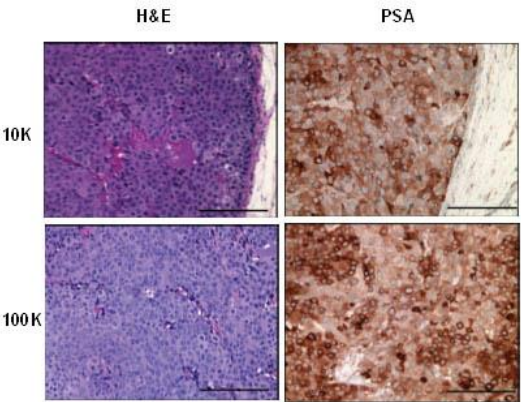
Figure 18. Histological analysis of LNCaP tumors. H&E stained sections of LNCaP tumors that formed in NOD/SCID mice when inoculated with 10,000 or 100,000 cells. Immunohistochemical stained sections of LNCaP tumors for PSA confirming expression of the biomarker in overt tumors.

Task 2. Response to chemotherapy and hormone therapy (Months 24-48).
2a. Inject traditional breast cancer cell-line based xenografts into mice using hormone receptor positive lines and hormone receptor negative and Her2+ lines (MCF7, T47D, HCC1418, SUM225, BT20, SUM149, SUM159)(Months 24-36). Human breast cancer cell lines are all commercially available and previously characterized. For more information/details on these cell line-based xenografts see: *Breast Cancer Research*, **2010**;12(5):1-17.

Cell-line based xenografts have been initiated and terminal blood collections have been made with MCF7, T47D and SUM1315 lines (N=10, 10, 12, respectively). Chemotherapy and hormone therapy treatments and studies have not yet been initiated.

2b. Allow tumors to form and reach 5mm and assess serum levels of EMT/CSC markers. (Months 24-36)
2c. Treat animals with chemotherapy (Paclitaxel/Taxol) or anti-estrogen (Tamoxifen) and measure serum levels of EMT/CSC markers and mtDNAs during tumor regression and after cessation of therapy.
2d. Continue to monitor tumor growth. (Months 36-48)
2e. Determine whether the levels of EMT/CSC markers correlate to response to therapy or to tumor recurrence (Months 36-48). Predicted Total mice =(30x2replicates)=60

These studies have not yet been initiated per SOW.

Task 3. Recurrence prediction (Months 36-60)
3a. Create tumors using the 'Human-In-Mouse' breast tumor model. Allow tumors to form and reach 5-8mm in diameter and assess serum levels of oncogenes used to create tumors (Months 36-50).
3b. Surgically resect the tumors and measure blood serum levels of EMT/CSC markers as well as mitochondrial DNAs during tumor regression and after cessation of therapy after surgery (Months 36-50).
3c. Monitor mice and measure the levels of EMT/CSC markers weekly to determine if they increase or correlate with regrowth of tumor (Months 48-60). Predicted Total mice=(80x2replicates)=160;Predicted total number of reduction mammoplasty tissues= 10

These studies have not yet been initiated per SOW.

Gail E. Sonenshein, Ph.D., *Tufts University School of Medicine 150 Harrison Avenue Boston, MA 02111*

Task 1. Perform mitochondrial DNA mutational analysis. (Months 1 to 16).

1a. Isolate mitochondria from cultured mouse and human mammary breast epithelial or cancer cells that exist in our laboratory and extract DNA and subject it to massively parallel sequencing and bioinformatics to identify mutations. (Months 1-8).
As mentioned in our previous annual report, we have developed the technologies and used these to characterize the mitochondrial DNA sequences in human and mouse cell lines and tumor tissue. Thus this task is essentially completed. However, as new inflammatory breast cancer (IBC) cell lines are established or as we acquire additional lines, we are analyzing their mtDNA sequences to increase our database.

1b. Isolate mitochondria from normal tissue and from tumors, extract DNA and subject it to massively parallel sequencing (Months 8-12).
We have developed methods to extract DNA from frozen and formalin fixed paraffin embedded (FFPE) tumor tissue. We have been able to successfully amplify DNA obtained from these tissues and are now

ready to analyze tumor tissue obtained from the HIM breast tumor model. In particular, we are working on SUM-1315 tumor tissue obtained from the Kuperwasser lab.

1c. Compare mtDNA from normal mouse mammary tissue and from tumor tissue using bioinformatics to identify mutations. (Months 10-16).
As mentioned in the previous annual report, to analyze mouse tissue, new primers were needed to selectively amplifying mouse mtDNA. We were previously having some difficulty in designing primers for mouse DNA as those reported in the literature produced large PCR products not amenable for sequencing. We have now identified and confirmed our new mouse specific primers and have started analyzing mouse DNA. We have begun our analysis on mtDNA from an MMTV-c-Rel mouse mammary parental line and from a derivative of this line following transformation by DMBA. We will next analyze DNA from transgenic mice developed in the Kuperwasser lab (Task 2a)

Task 2. Characterize mtDNA mutations resulting from oncogene expression in breast tumors (Months 16-24).

2a. Compare mtDNA from mammary tissue vs tumors or derived cell lines of transgenic mice driven by oncogenes implicated in breast cancer. Samples obtained from Kuperwasser (months 16-24)
We obtained unmatched serum and tissue samples from HIM tumors with SV40/*KRas* mutation from Kuperwasser lab. We are currently working on identifying mtDNA mutations induced by the *KRas* oncogene in the tumors and we will then look for these mutations in the serum samples. PCR products have been amplified from the *KRas* tumors as shown in **Figure 19**, and these have been sent for sequencing. We are also interested in determining whether BRCA1 carriers have particular mtDNA mutations. Breast tumors from patients with BRCA1 mutation are very difficult to detect by mammography and these patients are more susceptible to irradiation. Thus, we will first test DNA from mice carrying tumors with BRCA1 mutations. If characteristic mutations are seen, then patient DNA and blood samples will be assessed to determine whether a blood test for mtDNA mutations can be developed.
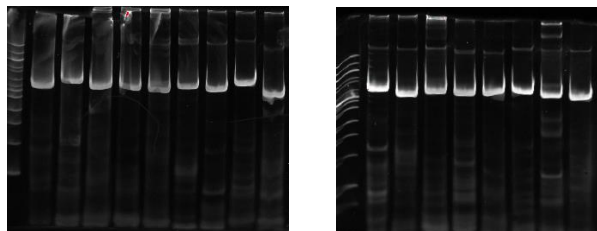
Figure19: DNA gel demonstrating clean amplification of mtDNA in the *SV40/KRas* tumors obtained from the Kuperwasser lab

2b. Characterize mtDNA alterations in tumor lines that will be utilized by the Kuperwasser laboratory in their 'HIM' analysis. DNA samples will be analyzed as in Task 1 above (Months 18-24).
We have obtained tumor tissue from the HIM tumors derived from the SUM1315 breast cancer cell line. DNA from these tissues has been amplified and is being analyzed using procedures described above.

Task 3. Recurrence prediction: Determine whether mtDNA mutations can be used to test for breast tumor regression in mice (in collaboration with Kuperwasser) (Months 18-60).

3a. mtDNA from tumor samples provided by the Kuperwasser laboratory using the HIM breast tumor model. Tumors will be initially removed after they have been allowed to reach 5-8 mm in diameter and then at the end of the experiment (Months 18-30)

We have developed the technology in our laboratory to perform tumor resection in mice. This technology will be used to assess whether mtDNA in the blood can be used to evaluate tumor regrowth/recurrence. Toward this end, we initiated a mouse study in which blood samples were obtained after tumor resection. NOD/SCID mice were injected with 2.5 x 10^6 MDA-MB-231 cells in the mammary fat pad. Mice were bled a day prior to injection and at day 7 and day 16 after cancer cell inoculation. The tumors were resected when they reached an average volume of 0.2 cm^3. Mouse 3 died before resection. As shown in **Table 2** below, tumor resection was successfully performed on 11 mice, which were then followed for a total of 32 days. Out of the 11 mice, 6 mice had primary recurrence over the 5-week period. All of the mice developed macro or micro metastases to the lung, including the ones that had no primary recurrence. Four of the mice developed brain metastases. We are currently using whole blood and tissue samples obtained from these mice to answer the following questions:

1. Can mtDNA be observed in mice (4, 9, 5 and 8) with early recurrence?
2. Can we observe mtDNA mutations in mice which developed lung and brain metastases but had no recurrence of their primary tumors (mice 7 and 10)?
3. Does the amount of mtDNA in the blood correlate with tumor burden and metastasis?

Table 2: This table depicts a summary of the resection experiment, including information on the specific mice that showed primary recurrence, brain metastases or lung metastases. +m: multiple metastases, +: single metastases, −: no metastases, ND: not determined. Most of the metastases observed in the brain were smaller micro metastases and those observed in the lung were macro metastases.

Mouse No#	# 1	# 2	#3 Died	# 4	# 5	# 6	#7	#8	#9	#10	#11	# 12
Primary recurrence	+ 3/20/14 17 days after resection	+ 4/03/14 33 days after resection		+ 3/7/14 4 days after resection	+ 3/7/14 4 days after resection	None	None	+ 3/14/14 11 days after resection	+ 3/7/14 4 days after resection	None	None	None
Brain metastasis	+m	+m		ND	+m	−	+	−	ND	−	−	−
Lung metastasis	+m	+		ND	+	+m	+	+	ND	+	+	+

3b. DNA will be isolated from serum collected before resection and weekly after resection that will be provided by the Kuperwasser laboratory (Months 18-30).

In our last annual report we successfully developed methods to isolate and amplify mtDNA from whole blood. Thus, we sought to determine the sensitivity of the mtDNA isolation and amplification procedures using mice bearing tumors of various sizes derived from MDA-MB-231 cells. Specifically, mice injected with 2.5 x 10^6 MDA-MB-231 cells in the mammary fat pad were bled on Day 7 when the tumors were only beginning to be palpable to verify our ability to isolate and detect mtDNA when tumor burden is low. In our analysis of these samples, we initially used random primers in the amplification, as these were successful in sequencing mtDNA from cell lines and tumors. However, we found that the amount of

human mtDNA obtained from 50-100 µL of whole blood per mouse was very low and inadequate to successfully amplify with these primers. Thus, we next tested and confirmed the use of specific primers for regions of the mtDNA in the sequencing reactions. Using this strategy, we successfully observed mtDNA mutations from the MDA-MB-231 cell-derived tumors in the blood of mice as early as Day 7 after injection in the mammary fat pad using primers that covered ~15-20 mtDNA mutations in the MDA-MB-231 cells. Thus, we can detect mtDNA in the blood of mice at a stage when the tumor is barely palpable, when circulating tumor cells (CTCs) are detectable [1]. The one drawback of this method, however, is that we would not amplify all of the mtDNA unless we use multiple specific overlapping primers that cover the entire circular DNA. Together these data suggest that mtDNA mutations can be used a marker for detection of early stage breast cancer recurrence in patients.

We are currently testing blood samples obtained from Kuperwasser lab from SUM1315 derived HIM tumors and are also looking for an increase in the frequency of mutations with tumor progression. However, the average serum volume size is less than 20 µl per time point and is insufficient for DNA extraction using our protocol. We have tried to pool some samples together from the same time point, but the DNA obtained has still been insufficient for PCR. Thus, we are currently exploring the Blood Phusion direct PCR kit (Thermo Scientific), which can amplify small amounts of DNA directly from blood without the need to isolate the DNA. Although this kit is designed for whole blood, we are currently optimizing it for use with serum. Also, as discussed above, we are currently testing whole blood samples obtained after resection from mice injected with MDA-MB-231 cells.

New Task. Identify critical miRNAs that are mediating invasive and metastatic phenotype driven by ADAM8

miRNA represent potential biomarkers for breast cancer detection as some are released from tumor cells and can be present stably in the blood stream. As described previously, we initiated a new Task aimed at identifying miRNAs regulated by ADAM8, which was not part of the original SOW, in order to elucidate new important breast cancer biomarkers for the Walt Lab to develop a detection assay. This Task has now been completed and a manuscript will be submitted shortly. Below is a summary of the work performed under this grant.

Our laboratory demonstrated that ADAM8 (**A D**isintegrin **A**nd **M**etalloprotease 8 protein) is a key downstream mediator of a RelB NF-κB pathway that promotes a more aggressive phenotype of breast cancer. ADAM8 belongs to a disintegrin and metalloprotease (ADAM) protein family, which mediate cell adhesion, migration, signaling and proteolysis of extracellular matrix. ADAM8 has four extracellular domains: a metalloproteinase (MP) domain involved in shedding and proteolysis of the matrix, a Disintegrin (DI) domain needed for β1-integrin activation and thereby adhesion to an endothelial layer, as well as a cysteine rich (CRD) and EGF-like (ELD) domain. We showed that *ADAM8* is overexpressed in breast tumor samples *vs* normal breast tissue, especially in ER-negative and triple-negative breast cancers. Importantly, *ADAM8* mRNA levels correlate with poor patient outcome, including metastatic relapse. Using immunohistochemistry, our collaborators in France have shown that 34% of triple negative tumors and 48% of breast metastases are positive for ADAM8 staining. In an orthotopic mammary mouse model, ADAM8 knockdown in MDA-MB-231 cells profoundly reduced tumor development, spreading of CTCs and metastases to the brain. Consistently, ADAM8 was shown to play an essential role in breast cancer cell migration, invasive outgrowth and anchorage-independent growth in breast cancer cells in culture.

4a. Identification of miRNAs regulated by ADAM8
As described in our previous report, we have identified 68 miRNAs regulated by ADAM8 and confirmed our initial miRNA candidate of interest miR-720 is induced and regulated by ADAM8 and secreted from breast cancer cells.

4b. Analysis of miR-720 in the ability of ADAM8 to promote an aggressive phenotype.

In our previous report we showed data that supports the hypothesis that miR-720 plays an important role in migration and invasive phenotype of these breast cancer cells, and that it is an important downstream mediator of ADAM8. We have now identified the signaling cascade that leads to the induction of miR-720. Specifically, we found that mutation in the MP active site failed to prevent miR-720 induction (**Figure 20A-B**). Furthermore, ADAM8 Remnant, which has the DI but not an MP domain, induced miR-720 essentially as effectively as WT ADAM8 (**Figure 20C-D**). Lastly, an antibody against ADAM8 or β1-integrin reduced miR-720 activation (**Figure 20E-F**). Overall, these findings indicate the DI domain of ADAM8 induces miR-720 via β1-integrin activation.
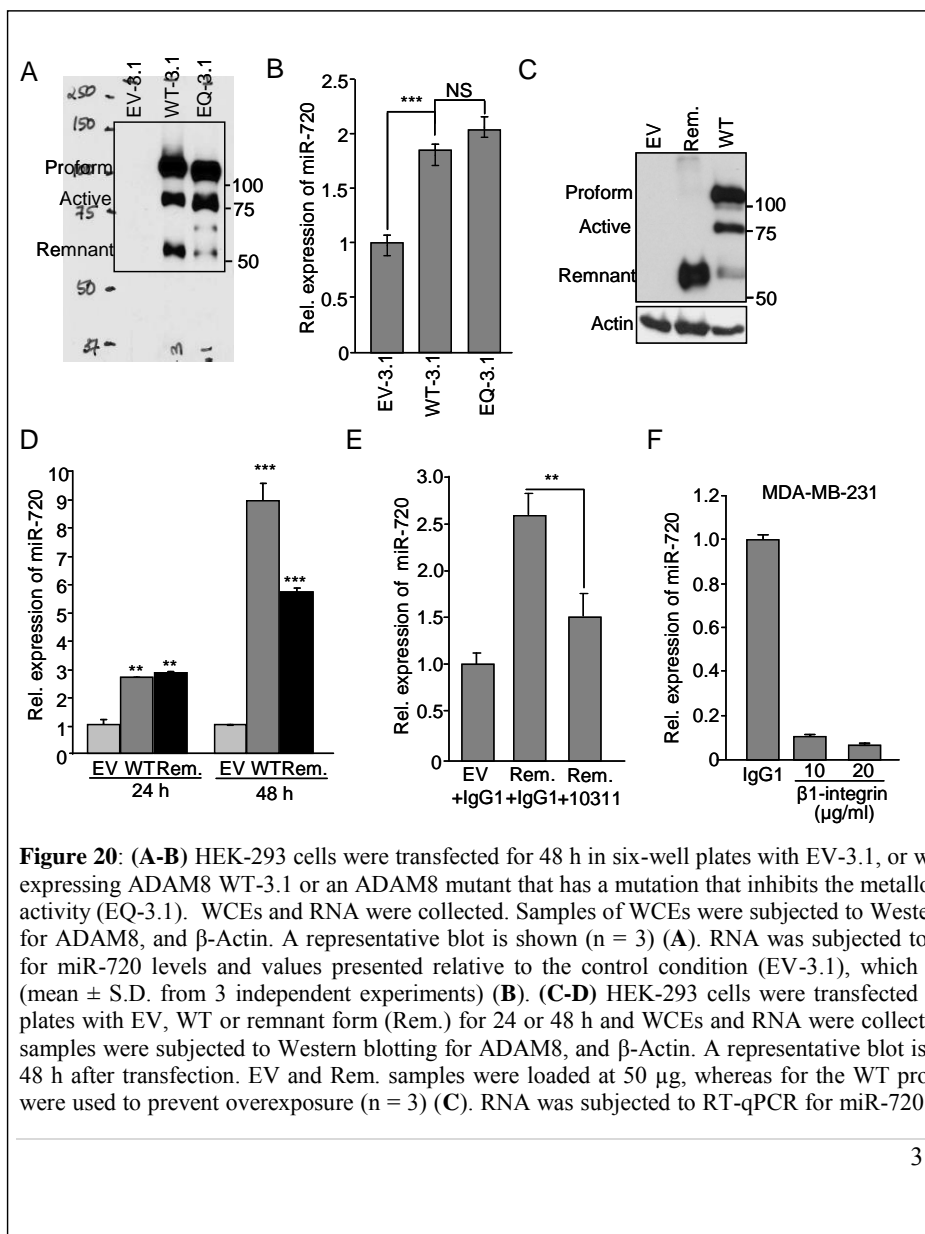
**Figure 20**: **(A-B)** HEK-293 cells were transfected for 48 h in six-well plates with EV-3.1, or with vectors expressing ADAM8 WT-3.1 or an ADAM8 mutant that has a mutation that inhibits the metalloproteinase activity (EQ-3.1). WCEs and RNA were collected. Samples of WCEs were subjected to Western blotting for ADAM8, and β-Actin. A representative blot is shown (n = 3) (**A**). RNA was subjected to RT-qPCR for miR-720 levels and values presented relative to the control condition (EV-3.1), which is set to 1 (mean ± S.D. from 3 independent experiments) (**B**). **(C-D)** HEK-293 cells were transfected in six-well plates with EV, WT or remnant form (Rem.) for 24 or 48 h and WCEs and RNA were collected. Protein samples were subjected to Western blotting for ADAM8, and β-Actin. A representative blot is shown for 48 h after transfection. EV and Rem. samples were loaded at 50 μg, whereas for the WT protein 10 μg were used to prevent overexposure (n = 3) (**C**). RNA was subjected to RT-qPCR for miR-720 levels. EV

control condition is set to 1 (mean ± S.D. from 3 independent experiments) (**D**). **E**) HEK-293 cells were transfected in 12-well plates with a vector expressing the Rem. using Lipofectamine 2000. After 24 h, the transfected cells were treated with 20 µg/ml of ADAM8 antibody targeting the DI/CRD domains (10311), or control isotype (IgG1) for another 24 h and RNA was extracted. RT-qPCR analysis was performed to measure miR-720 levels. Control condition (EV+ IgG1) is set to 1 (mean ± S.D. from 3 independent experiments). **F**) MDA-MB-231 cells were treated with 10 or 20 µg/ml of β-1 integrin antibody, or isotype-matched control IgG2A for 24 h and RNA subjected to RT-qPCR analysis for miR-720. Control condition (IgG2A) is set to 1 (mean ± S.D. from 3 independent experiments). *P < 0.05, **P < 0.01, ***P < 0.001 Student's t-test.

4c. Detection of miR-720 in the blood of tumor bearing mice.

In our previous report, we discussed two substantial challenges in our attempts to analyze miR-720 levels in the blood: (1) obtaining sufficient amounts of RNA from less than 50 µl of serum and (2) identifying a good normalization RNA to control for variability between the serum samples. These challenges have now been overcome. We have discovered that using the Exiqon miRcury RNA isolation kit for biofluids for the RNA isolation yields adequate amounts of RNA. We have also ascertained that addition of a low amount of *C. elegans* miR-39 (1X 10^8 copies/uL) as a spike control allows us to use it for normalization. Using these new approaches, we have been able to detect miR-720 in the plasma of mice bearing tumors derived from MDA-MB-231 cells as early as 7 days after cancer cell inoculation. Furthermore while we only have small numbers of mice, the amount of miR-720 present in the blood at this early time point appears to correlate with the aggressive nature of the tumor. For example, the mice with the most aggressive, fast growing tumors (mouse 5 and mouse 3) also have the highest amount of miR-720 in the plasma when the tumor is barely palpable. Taken together these results indicate that miR-720 might be a good predictive biomarker for early discovery of aggressive triple negative breast cancer.

A   B
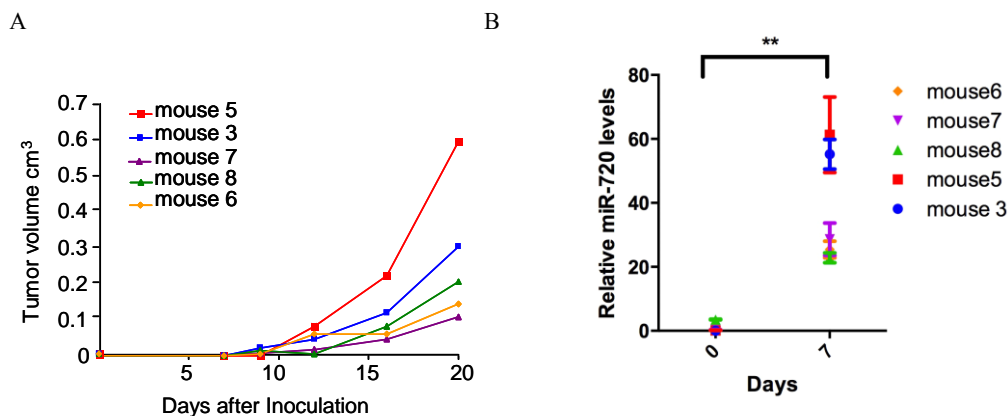
Figure 21: A) Tumor volume measured over a period of Days B) Relative miR-720 levels in plasma obtained from mice bearing tumors derived from MDA-MB-231 cells at Day 0 and Day 7.

In summary, in the last year we have successfully completed our mouse experiment and identified samples from specific mice that can be used to answer important questions about the detection of mtDNA mutations during tumor progression and recurrence. We are also optimizing a method to perform direct PCR from small quantities of serum using the Blood Phusion direct PCR kit. During the next year- we will be working closely with the Kuperwasser group to analyze mtDNA in early stages of tumor

progression, such as DCIS and hyperplasia, as well as in advanced tumors and in mice that show recurrence. We have also completed our miRNA study and shown that miRNA's regulated by ADAM8 such as miR-720 have potential as biomarkers for early detection of triple negative breast cancer.

Buchsbaum Laboratory—Tufts Medical Center

Section 1- A brief introduction covering the purpose and scope of the research effort.

The research effort includes both laboratory and clinical research aims. The purpose of the laboratory effort is to determine the effect of the tumor microenvironment on serum markers of metastasis in the HIM model. The purpose of the clinical research effort is to validate the serum markers of metastasis derived from the Walt and Chiu pre-clinical experiments using human serum samples.

Section II - A brief description of overall progress to date plus a separate description for each task or other logical segment of work on which effort was expended during the report period. Description shall include pertinent data and graphs in sufficient detail to explain any significant results achieved. If this award includes the recruitment of human subjects for clinical research or a clinical trial, report progress on subject recruitment (i.e., number of subjects enrolled versus total number proposed).

Task 1. Determine effect of tumor microenvironment on serum markers of metastasis in the HIM model (Months 1-36).

1a. Develop mammary fibroblast lines with range of Tiam1 (both down- and up-regulated). (Months 1-6)

Completed as detailed in prior reports.

1b. Utilize HIM breast tumor model in collaboration with Dr. Kuperwasser.
Task 1. In the prior Annual Progress Report we summarized our analysis of the effects of Tiam1-manipulated fibroblasts in the 3D in vitro breast cancer microenvironment, as well as two mouse models of human breast cancer metastasis. We also showed initial results using a chemical inhibitor to the Tiam1-deficiency pathway and its effect in blocking metastasis in the second mouse model. In this model, the mice receive xenografts with breast cancer cells isolated from 3D co-cultures after exposure to engineered mammary fibroblasts. In the original protocol we used this inhibitor to treat 3D tissue cultures, prior to xenograft implantation in the mice.

During this year we have initiated a modification to the second mouse model of human breast cancer metastasis. In the new modified model, mice are treated directly with the inhibitor, rather than treating the co-cultures with the inhibitor. To do this, we worked with our supplying collaborator to derive a suitable supply of the inhibitor. We applied for and received approval from our institutional DLAM to amend our current animal protocol to permit this treatment. We initiated the 3D tissue cultures necessary for the implantation experiments, and have treated sixteen additional mice have now been treated on this modified protocol. All mice developed primary tumors at the site of implantation, and tolerated the direct treatment, which consisted of daily i.p. injections beginning approximately two weeks after implantation (once staples were removed). Mice have been sacrificed, tumors and organs harvested, and pathologic studies are pending. Terminal serum specimens were obtained on all mice.
We also continued in vitro studies on six additional related compounds to test potential inhibitory ability against the Tiam1-deficiency pathway, with variable results in initial biochemical testing requiring multiple repetitions of experiments to ensure accuracy. After standardizing procedures and increasing personnel expertise, we have completed the initial biochemical testing of six additional compounds. These results have identified one of the six new compounds as a potential novel inhibitor with greater

efficacy and less toxicity in vitro than the initial inhibitor. We are currently conducting expanded dose titration experiments in vitro to establish optimal conditions for testing this new compound in functional studies based on the 3D culture model. Once these are completed we anticipate testing the new compound in the mouse xenograft models.

Task 2. Perform retrospective clinical trial to validate candidate markers from Walt single molecule studies using banked repository samples. (Months 1-60)

During this period we have worked with statisticians in the Tufts Research Design Center within the Tufts Clinical and Translational Sciences Institute to define needed numbers of human serum samples for testing of the initial biomarker panel, based on prevalence estimates derived from reports of circulating tumor cells.

We have also identified potential samples within the NIH PLCO (Prostate, Lung, Colorectal and Ovarian) Cancer screening trial. In particular this trial includes samples from women prior to development of breast cancer, which are otherwise very difficult to find in suitable number and sample volume. A Concept Application has been submitted to the PLCO as the initial step in the process for access to the samples, based on recent data from the Walt and Kuperwasser labs derived from proof-of-concept experiments demonstrating the ability to detect circulating PSA in mice implanted with human prostate cancer cells prior to the development of measurable tumors. Based on feedback to the Concept Application we anticipate submitting a full application to the PLCO at the new open application period (December).

Task 3. Perform prospective clinical trial for predictive and prognostic markers in women with newly diagnosed breast cancer.

Progress on developing a bank of human serum samples for validation of candidate markers is continuing. The goal is to bank serum samples from all women with newly diagnosed breast cancer, women who are being followed after completing treatment for localized breast cancer, and women with active metastatic breast cancer being treated at Tufts Medical Center. Particular focus has been on banking serum from women with newly diagnosed breast cancer, prior to definitive surgery, as these samples are not generally available from outside serum collections. Recruitment of consenting subjects and serum samples to our Tissue Repository is currently ongoing. During this period we have also successfully recruited other clinicians, most importantly breast cancer surgeons and breast center personnel, to this effort. This has led to a significant increase in consenting subjects and sample collections (25 specimen collections in the past two months alone). However, the increase in sample collection has exposed logistical issues in the process of handling specimens in the main laboratory prior to delivery to the Tissue Repository, and efforts at process improvement are underway.

Task 4. Obtain clinical tumor samples for single cell analysis to determine tumor composition (see Walt task 3) and analysis of mtDNA (see Sonenshein task 4). (Months 1-60)

These studies have not yet been initiated per SOW

KEY RESEARCH ACCOMPLISHMENTS

-   Developed SiMoA assays for TBX3 (LOD=1.7 fM), CA 15-3 (LOD=0.001 U/mL), CDKN2D (LOD=5.7 fM), BORIS (LOD=280 fM), ADAM12 (LOD=55 fM), HER2 (LOD= 2.2 fM), PR (LOD=1.5 fM), ER-α (LOD=2.4 fM), MCP-1 (LOD=7 fM), CYR61 (LOD=0.3

fM), LCN2 (LOD=19 fM), SERPINE2 (LOD=864fM), CA 19-9 (LOD=0.76 U/mL) and NEDD9 (LOD=174fM).
- Performed preliminary studies to quantify candidate biomarker levels in healthy and diseased human serum and evaluate usefulness of each marker.
- Established a method to isolate single cells for SiMoA assays.
- Measured the PSA content from over 45 single LNCaP cells.
- Completed validation of a low-throughput method for the manipulation of single cells for digital assays, and developed a new technique with potential for the high-throughput parallel manipulations of single cells using bipolar electrode based dielectrophoresis.
- Isolated CTCs from breast cancer patients, and characterized the limit of detection of eDAR.
- Developed strategies for increasing the number of CTCs isolated from breast cancer patients.
- Developed a new eDAR device for the simultaneous and selective isolation of multiple subpopulations of CTCs.
- Developed and validated a method for the digital PCR analysis of single cancer cells.
- Established modified model of metastasis in HIM model and obtained terminal bleeds.
- Identified new compound with increased potency against metastasis and decreased toxicity based on in vitro assays.
- Identified available serum bank through NIH PLCO screening trial and submitted initial Concept Application.
- Established active process for recruiting consenting subjects to donate serum for banking at Tufts Medical Center.

REPORTABLE OUTCOMES

- Schubert, S.M.; Arendt, L.; Zhou, W.; Baig, B.; Walter, S.R.; Kuperwasser, C.; Walt, D.R. Early Detection of a Cancer Biomarker in Mice Using Ultra-sensitive Protein Detection. Manuscript Submission.
- Baig, S., Schubert, S. M., Walter, S.R., Walt, D. R. Development of Ultra-Sensitive Assays for Early Breast Cancer Detection and Single Cell Analysis. Oral presentation for Tufts University Breast Cancer Working Group; 2014 April 28, Boston, MA.
- Walter, S.R., Schubert, S. M., Baig, S., Walt, D. R. Ultrasensitive Detection of Breast Cancer Biomarkers and Single Cell Protein Analysis. Oral talk and poster presented at: Bioanalytical Sensors GRC; 2014 June 26; Newport, RI.
- Baig, S., Schubert, S. M., Walter, S.R., Walt, D. R. Development of Ultrasensitive Protein Assays for the Early Detection of Breast Cancer. Poster presented at: Bioanalytical Sensors GRC; 2014 June 21; Newport, RI.
- M. Zhao, B. Wei, D.T. Chiu (2013) "Imaging multiple biomarkers in eDAR captured rare cells with sequential immunostaining and photobleaching" *Method Methods* 64, 108-113.
- M. Zhao, W.C. Nelson, B. Wei, P.G. Schiro, B.M. Hakimi, E.S. Johnson, R.K. Perdue, G. Gyurkey, L.M. White, S. Whiting, D.T. Chiu (2013) "New generation of ensemble-decision aliquot ranking based on simplified microfluidic components for large-capacity trapping of circulating tumor cells" *Anal. Chem.* 85, 9671-9677.
- Y. Rong, J. Yu, X. Zhang, W. Sun, F. Ye, I. Wu, Y. Zhang, S. Hayden, Y. Zhang, C. Wu and D.T. Chiu (2014) "New yellow fluorescent semiconducting polymer dots with high brightness, small size and narrow emission for biological applications" *ACS Macro Lett.* 3, 1051-1054.

- M. Zhao, B. Wei, W.C. Nelson, D.T. Chiu (2014) "Simultaneous and selective isolation of multiple subpopulations of rare cells from peripheral blood using ensemble-decision aliquot ranking" (submitted).
- A.M. Thompson, A. Gansen, A.L. Paguirigan, J.E. Kreutz, J.P. Radich, D.T. Chiu (2014) "The self-digitization microfluidic chip for the absolute quantification of mRNA in single cells" (submitted).
- (6) R.K. Anand, E.S. Johnson, D.T. Chiu (2014) " Negative dielectrophoretic capture and repulsion of single cells at a bipolar electrode: the impact of faradaic ion en-richment and depletion" (submitted).
- Schubert, S. M., Baig, S., Walter, S.R., Walt, D. R. The Development of Serum-Based Single Molecule Assays for Early Detection of Cancer. Poster presented at: Single Molecule Approaches to Biology GRC; 2014 July 15 & 17th; Lucca (Barga), Italy
- Schubert, S. M., Baig, S., Walt, D. R. Single Molecule Assays for Early Breast Cancer Detection. Poster presented at: Pittsburgh Conference; 2014 March 3; Chicago, IL.
- Sonenshein, G. E., "Identification of miR-720, as a downstream target of ADAM8 promoting migratory and invasive phenotype in triple negative breast cancer" (ready for submission)

CONCLUSION

In summary, we have developed a high-sensitivity and high-throughput method called eDAR for the isolation of cell biomarkers (CTCs) for breast cancer prognosis. We have a low-throughput manual method for analyzing these cells with digital assays (e.g. digital PCR), and have explored a new high-throughput method for manipulating many single cells in parallel using bipolar electrode based dielectrophoresis. With these methods, we have begun to isolate CTCs from breast cancer patients. We found CTCs from patients to be highly heterogeneous in terms of the amount and type of cell-surface markers they present. To address this, we have used a cocktail of antibodies to help improve the isolation of CTCs. We have also developed an eDAR chip capable of isolating different subpopulations of CTCs.

Great progress was made in the development of SiMoA assays for the targeted breast cancer biomarkers. A total of 13 SiMoA assays have now been successfully completed, most with LODs significantly lower than their commercial ELISA counterpart. Although some of these assays can still be optimized to gain more sensitivity, more focus will be placed on utilizing these assays for determining biomarker concentrations in breast cancer patient samples. We have also begun preliminary screening of multiple biomarkers in breast cancer patient and healthy control samples. Although additional samples must be screened to gain greater statistical information and further data processing is required, our preliminary results seem promising.

In addition, we have established a mouse model to highlight the use of SiMoA for the early detection of cancer. This proof-of-concept study using PSA demonstrated that biomarkers can be measured at ultrasensitive levels within serum using SiMoA prior to tumor formation. These results are vital to the implementation of SiMoA technology as an early detection and monitoring platform for breast cancer.

We have successfully achieved full quantification of protein molecules within single cancer cells using SiMoA. Highly cultured cells were found to exhibit different protein expression levels than low-passage cells. This technique will be applied to quantify protein copy numbers in single breast cancer cells using several of the established SiMoA assays described above.

REFERENCES

(1)   *Breast Cancer Facts & Figures 2013-2014*; American Cancer Society, Inc.: Atlanta, 2013.
(2)   Rice, J. *Nature* **2012**, *485*, S55.
(3)   Taplin, S.; Abraham, L.; Barlow, W. E.; Fenton, J. J.; Berns, E. A.; Carney, P. A.; Cutter, G. R.; Sickles, E. A.; Carl, D.; Elmore, J. G. *J Natl Cancer Inst* **2008**, *100*, 876.
(4)   Jørgensen, K. J.; Gøtzsche, P. C. *BMJ* **2009**, *339*.
(5)   Giljohann, D. A.; Mirkin, C. A. *Nature* **2009**, *462*, 462.
(6)   Ballehaninna, U. K.; Chamberlain, R. S. *Journal of gastrointestinal oncology* **2012**, *3*, 105.
(7)   Fayard, B.; Bianchi, F.; Dey, J.; Moreno, E.; Djaffer, S.; Hynes, N. E.; Monard, D. *Cancer Res.* **2009**, *69*, 5690.
(8)   Candia, B.; Hines, W.; Heaphy, C.; Griffith, J.; Orlando, R. *Cancer Cell International* **2006**, *6*, 16.
(9)   Tikhmyanova, N.; Tulin, A. V.; Roegiers, F.; Golemis, E. *PLoS ONE* **2010**, *5*, e12369.
(10)   Little, J. L.; Serzhanova, V.; Izumchenko, E.; Egleston, B. L.; Parise, E.; Klein-Szanto, A. J.; Loudon, G.; Shubina, M.; Seo, S.; Kurokawa, M.; Ochs, M. F.; Golemis, E. A. *Oncogene* **2014**, *33*, 411.
(11)   Wilson, D. H.; Hanlon, D. W.; Provuncher, G. K.; Chang, L.; Song, L.; Patel, P. P.; Ferrell, E. P.; Lepor, H.; Partin, A. W.; Chan, D. W.; Sokoll, L. J.; Cheli, C. D.; Thiel, R. P.; Fournier, D. R.; Duffy, D. C. *Clinical Chemistry* **2011**, *57*, 1712.
(12)   Romagnoli M, Mineva ND, Polmear M, Conrad C, Srinivasan S, Loussouarn D, Braille-Nion S, Georgakoudi I, Dagg A, McDermott EW *et al*: ADAM8 expression in invasive breast cancer promotes tumor dissemination and metastasis. *EMBO Mol Med* 2014, 6(2):278-294.